

Stochastic Diagrams for Critical Point Spectra

S. Chaturvedi* and P. D. Drummond

Department of Physics, University of Queensland
St Lucia 4067, Queensland, Australia.

February 1, 2008

Abstract

A new technique for calculating the time-evolution, correlations and steady state spectra for nonlinear stochastic differential equations is presented. To illustrate the method, we consider examples involving cubic nonlinearities in an N -dimensional phase-space. These serve as a useful paradigm for describing critical point phase transitions in numerous equilibrium and non-equilibrium systems. The technique presented here is not perturbative. It consists in developing the stochastic variable as a power series in time, and using this to compute the short time expansion for the correlation functions. This, in turn, is extrapolated to large times and Fourier transformed to obtain the spectrum. A stochastic diagram technique is developed to facilitate computation of the coefficients of the relevant power series expansion. Two different types of long-time extrapolation technique, involving either simple exponentials or logarithmic rational approximations, are evaluated for third-order diagrams. The analytical results thus obtained are compared with numerical simulations, together with exact results available in special cases. The agreement is found to be excellent up to and in the neighborhood of the critical point. The exponential extrapolation works especially well even above the critical point at large N -values, where the dynamics is one of phase-diffusion in the presence of a spontaneously broken symmetry. A feature of this method is that it also enables the calculation of the steady state spectra of polynomial functions of the stochastic variable. In these cases, the final correlations can be non-bistable even above threshold, and the logarithmic rational extrapolation has the greater accuracy. Finally, we emphasize that the technique is also applicable to more general stochastic problems involving spatial variation in addition to temporal variation.

*Permanent address : School of Physics, University of Hyderabad, Hyderabad 500046
(India)

1 Introduction

Stochastic differential equations are a natural way of describing the interaction of a system with a random reservoir. They were introduced by Langevin[1] to help explain Einstein's theory[2] of small particles immersed in a fluid, as observed by the biologist Robert Brown. More rigorous mathematical treatments were later introduced by Ito[3] and Stratonovich[4]. They have now diffused into many different areas[5] of physics, chemistry and biology. In recent times, similar models have been utilized in ever more diverse fields, including engineering, economics[6] , and even sociology. The essence of a stochastic differential equation is that it isolates a system of interest from the background of random events that may influence the system. Implicit in this formulation is the idea that the reservoir, or source of random fluctuations, evolves without reference to the system of interest. This simplifies the study of otherwise complex coupled phenomena.

As an example, the calculation of correlation functions, and hence the spectra, of physical systems near phase transitions is of considerable theoretical interest. These have dynamical properties that are often conveniently described using stochastic differential equations. However, commonly used analytic techniques like linearization, frequently become invalid near phase-transition points. At the same time, while numerical simulation is possible, this is a time-consuming computational procedure without resulting in a great deal of insight. Thus, there is a need for techniques that give analytical results. Rather surprisingly, there are few systematic procedures for treating nonlinear stochastic differential equations under conditions where linearization is invalid.

In this paper we consider the spectra of physical systems that are described by stochastic differential equations near a critical point phase transition. Such differential equations have a near universal applicability, both for equilibrium and non-equilibrium phase transitions [5]. For instance, they arise in theoretical treatments of single mode lasers [5], inhomogeneously and homogeneously broadened two mode lasers [7, 9], and optical parametric amplifiers near threshold [10, 11]. A number of useful theoretical techniques [12, 17] are known for these problems, some of which improve upon the the conventional Zwanzig-Mori projection operator method [18, 19]. However, these techniques are cumbersome for systems in higher phase space dimensions.

Instead, we propose a simple, direct calculation which is based on the stochastic differential equation. The resulting integral expressions can be classified diagrammatically, in a way that allows a straightforward calculation of essential combinatoric factors. The results give a power series in time which can be extrapolated to long times with reasonable accuracy in many cases. We analyze two possible extrapolation techniques, namely the exponential of a rational function, and a series of simple exponential terms. Either method gives excellent results at or below the critical point.

Above the critical point, we find differences in accuracy, and this can be

related to the dominant eigenvalue distributions for different types of equation and observable. Convergence is slowest when the spectrum has characteristic time-scales which are an exponential function of an equation parameter, as in the one-dimensional cubic stochastic process above threshold, which involves diffusion over a barrier. The exponential series method is preferable for simple types of spectra with only one or two dominant eigenvalues, which turns out to be the case for the N -dimensional cubic stochastic process at large N -values. The rational function method is best for complex spectra without much range in characteristic time-scales. An example of this is the intensity (x^2) correlation spectrum of the one-dimensional cubic process, which can be represented with remarkable accuracy using low-order rational function extrapolation.

More generally, we expect that this method can be applied to any stochastic differential equation where conventional linearization methods are inapplicable due to large nonlinear terms. Under these circumstances, it may be useful to have a nonlinear solution of the type derived here, as a starting point for a perturbative or asymptotic analysis. For these reasons, it is useful to analyze the simple cubic nonlinear case in detail, both as a test case for the stochastic diagram method, and as an elementary stochastic process of intrinsic interest.

2 Stochastic Equations

The method of stochastic diagrams to calculate solutions to stochastic differential equations is normally applied in the frequency domain, where it corresponds to a perturbation theory expansion in a small coupling constant [20, 21]. In these applications, there is a close resemblance to Feynman diagram techniques. In both cases, the starting point of the iterative method is the approximate linearized solution to the problem, which becomes the solution to the entire correlation function in the limit as the coupling constant approaches zero. Frequency domain stochastic diagrams have many useful applications, including the stochastic quantization approach to quantum field theory. An essential difference between these methods and Feynman diagrams, is the appearance of stochastic terms that are averaged over at a later stage.

We choose here to apply stochastic diagrams to the time domain correlation function. This has the advantage that there are no singularities in the series expansion coefficients, even at a critical point. A corresponding disadvantage is that the long time correlation functions cannot be directly calculated, and must be approximated by an extrapolation procedure that is based on some known property of the solution. In the examples given here, we use either simple exponentials or logarithmic rational function extrapolation, which results in analytic expressions for the approximate correlation function. A direct comparison with numerically calculated spectra will be used to demonstrate the great accuracy of this procedure in calculating spectra near critical points. It is less accurate above threshold in the bistable cases where stochastic ‘barrier hopping’ or ‘tun-

neling' can occur, resulting in widely differing eigenvalues. This results in a reduced precision for the extrapolation. Methods based on multiple time scales can be used in these cases.

Surprisingly, in the closely related higher-dimensional phase-diffusion problem, stochastic diagrams give good results. An example of this is the laser above threshold. This is because the long time-scale here is not exponentially long, as it is in the tunneling cases. Good results are also found for non-bistable variables like the intensity, even when the underlying equations are themselves bistable. This is because the extrapolation is carried out in terms of the correlation function, which has a different behavior to the underlying stochastic variable. In order to illustrate these various cases, we start with a very general form of stochastic differential equation.

The equations we wish to treat are of the form

$$\dot{\mathbf{x}} = \mathbf{A}(\mathbf{x}) + \mathbf{B}(\mathbf{x}) \cdot \boldsymbol{\xi}(t) \quad , \quad (1)$$

where the real noise sources $\xi_i(t)$ have zero mean and are delta-correlated in time so that

$$\langle \xi_i(t) \rangle = 0 \quad ; \quad \langle \xi_i(t) \xi_j(t') \rangle = \delta_{ij} \delta(t - t') \quad . \quad (2)$$

Here \mathbf{x} is a real vector of n -dimensions, \mathbf{A} is an n -dimensional real polynomial vector function of \mathbf{x} and \mathbf{B} is an $n \times m$ dimensional real polynomial matrix function of \mathbf{x} . The vector $\boldsymbol{\xi}(t)$ is an m -dimensional real Gaussian stochastic process, interpreted in the Itô sense[22], for computational simplicity.

2.1 Iterative solutions

The method of stochastic diagrams consists of performing an iterative solution for $\mathbf{x}^{(p)}(t)$ so that

$$\mathbf{x}^{(p)}(t) = \mathbf{x}_0 + \int_{t_0}^t dt' [\mathbf{A}(\mathbf{x}^{(n-1)}(t')) + \mathbf{B}(\mathbf{x}^{(n-1)}(t')) \cdot \boldsymbol{\xi}(t')] \quad , \quad (3)$$

where $\mathbf{x}^{(0)}(t) \equiv \mathbf{x}_0 \equiv \mathbf{x}(t_0)$. Next, correlation functions of the typical form

$$\mathcal{G}_{ij}(t, t_0) = \langle x_i(t) x_j(t_0) \rangle - \langle x_i(t) \rangle \langle x_j(t_0) \rangle \quad , \quad (4)$$

are evaluated to p^{th} order, resulting in an expansion of $\mathcal{G}_{ij}(t, t_0)$ as a power series in $\tau = t - t_0$ for $\tau > 0$. For any given term p in the power series, iterations must be carried out until all possible terms in τ^p are evaluated. The result of the iterations consists of integrals over time which will be represented as directed lines in the stochastic diagrams. In addition, there are polynomials in variables (represented as vertices), initial conditions in the variables (represented as terminating arrows, and treated as delta functions at the initial time) and stochastic terms (represented as crosses).

2.2 Cubic stochastic process

Thus, for example, the solution of the well-known cubic stochastic process [22]

$$\dot{x} = -x^3 + \xi(t) \quad , \quad (5)$$

has a first iteration, starting from a known initial value $x(0) = v$ at $t = 0$, of

$$x^{(1)}(t) = v + w(t) - \int_0^t dt' v^3 \quad . \quad (6)$$

where $w(t) = \int_0^t dt' \xi(t')$. More generally, the n^{th} iteration in this simple one-dimensional case is written

$$x^{(n)}(t) = v + w(t) - \int_0^t dt' (x^{(n-1)}(t'))^3 \quad . \quad (7)$$

Thus, we can expand the second term in the iteration as

$$\begin{aligned} x^{(2)}(t) &= v + w(t) - \int_0^t dt' [v + w(t') - t' v^3]^3 \\ &= v + w(t) + \int_0^t dt' [(t')^3 v^9 - 3(t')^2 v^6 w(t') - 3(t')^2 v^7 - 6t' v^4 w(t') \\ &\quad + 3t' v^3 w(t')^2 + 3t' v^5 - w(t')^3 - 3v^2 w(t') - 3v w(t')^2 - v^3] \quad . \end{aligned} \quad (8)$$

We see that even this simple example leads to a large number of distinct terms, which need to be classified in a systematic way. In particular, while the leading term in the integral is of order t^4 , there are other terms of lower order present, including the stochastic terms and a term of order t which comes from the initial condition.

2.3 Stochastic diagrams

The next term in the iteration involves a cubic integral of $x^{(2)}(t)$, and clearly the combinatoric factors involved are more complex to three and higher orders. In order to simplify the counting of these factors, a diagrammatic classification can be introduced at this stage. In this classification, the terms are given diagrammatically to first order in Fig (1). To second order, all possible terms in $x^{(1)}(t)$ appear as ‘legs’ on the nonlinear vertex, to the next higher order, as shown in Fig (2).

Not all terms will contribute to the same order in a power series in τ , since the expectation value of a product of two stochastic integrals is proportional to τ , while the product of two deterministic integrals is proportional to τ^2 . This means that a reordering of the sequence is needed, to obtain a series of terms to a given order in τ . The rules are simple: all vertices counts as one order in

τ while stochastic terms count as half an order in τ and initial values as zero order. If the terms in the reordered series are labeled as $\tilde{x}^{(n)}(t)$ we can represent them according to Fig (3). On expanding all the relevant terms in Fig (3), we obtain:

$$\begin{aligned}
\tilde{x}^{(0)}(t) &= v \\
\tilde{x}^{(1/2)}(t) &= w(t) \\
\tilde{x}^{(1)}(t) &= -v^3 t \\
\tilde{x}^{(3/2)}(t) &= -3v^2 \tilde{w}(t) \\
\tilde{x}^{(2)}(t) &= 3[-v\tilde{w}^2(t) + v^5 t^2/2] \\
\tilde{x}^{(5/2)}(t) &= -\tilde{w}^3(t) + 9v^4 \int_0^t \tilde{w}(t') dt' + 6v^4 \int_0^t w(t') t' dt' \\
\tilde{x}^{(3)}(t) &= 3v^3 \int_0^t w^2(t') t' dt' + 9v^3 \int_0^t \tilde{w}^2(t') dt' \\
&\quad + 18v^3 \int_0^t w(t') \tilde{w}(t') dt' - t^3 v^7 - \frac{3}{2} t^3 v^7. \tag{9}
\end{aligned}$$

Here we have introduced the notation of:

$$\tilde{w}^n(t) \equiv \int_0^t w^n(t') dt'. \tag{10}$$

Further rules in stochastic calculus (of the Itô variety) are that the expectation values of the products of initial terms with stochastic terms decorrelate to all orders at later times and all odd products of stochastic integrals average to zero. This means that the only surviving terms in the expectation value \mathcal{G}_{ij} must be the terms of integer order in the series. For other types of expectation values (involving polynomials in $x(t)$), these extra terms must be retained.

If we take expectation values of the relevant stochastic terms, they have the structure:

$$\begin{aligned}
\langle w^2(t) \rangle &= t \\
\langle \tilde{w}(t) w(t) \rangle &= \langle \tilde{w}^2(t) \rangle = t^2/2. \tag{11}
\end{aligned}$$

Hence, on decorrelating, integrating over time, and combining all the relevant terms up to third order we obtain (for the average and correlation function of $x(t)$):

$$\begin{aligned}
\langle x(t) \rangle &= \langle v - tv^3 + \frac{3}{2}t^2(v^5 - v) + \frac{1}{2}t^3(11v^3 - 5v^7) \rangle \\
\langle x(t)x(0) \rangle &= \langle v^2 - tv^4 + \frac{3}{2}t^2(v^6 - v^2) + \frac{1}{2}t^3(11v^4 - 5v^8) \rangle. \tag{12}
\end{aligned}$$

These results are valid for an arbitrary initial distribution function. If carried out to higher orders, it is clear that they can describe either a transient process, or else a steady-state correlation in the time-domain, to any order in time.

3 N-dimensional cubic stochastic process

Having introduced the stochastic diagram method, we now apply it to the N-dimensional cubic stochastic process

$$\dot{x}_i(t) = -\eta_i x_i - f_{ijkl} x_j x_k x_l + \xi_i(t) \quad ; \quad i, j, k, l = 1, \dots, N \quad . \quad (13)$$

Here summation over repeated indices is implied. The coefficient f_{ijkl} of the cubic terms can be taken to be symmetric in the the last three indices without any loss of generality. This stochastic equation, with appropriate choice of parameters accommodates the stochastic equations that have been considered in the context of single and two mode lasers and optical parametric amplifiers [1-6]. The quantities of interest are the equilibrium correlation functions

$$\mathcal{G}_{ij}^{(n)}(\tau) = \lim_{t_0 \rightarrow \infty} [\langle x_i^n(\tau + t_0) x_j^n(t_0) \rangle - \langle x_i^n(\tau + t_0) \rangle \langle x_j^n(t_0) \rangle] \quad . \quad (14)$$

This equation now has the added feature of a linear loss/gain term η . When $\eta > 0$, there is additional damping, and the system is below threshold in the usual sense. The deterministic critical point is at $\eta = 0$. When $\eta < 0$, the system has linear gain (like a laser above the lasing threshold), and the system is then above the critical point. However, it is worth noting that as the dimensionality increases, this type of classification which comes from a linearized analysis is rather misleading. In fact, the enlarged phase-space volume means that noise sources become increasingly important at large dimensionality - to the point that there is a reduced distinction between the above and below threshold cases.

3.1 Steady-state behavior

Steady-state behavior is most readily analyzed if, for simplicity, we confine ourselves to the following equation with N -dimensional rotational symmetry:

$$\dot{\mathbf{x}}(t) = -\eta \mathbf{x} - \mathbf{x}(\mathbf{x} \cdot \mathbf{x})/N + \boldsymbol{\xi}(t) \quad . \quad (15)$$

This corresponds to defining the cubic coefficient as: $f_{ijkl} = [\delta_{ij}\delta_{kl} + \delta_{ik}\delta_{jl} + \delta_{il}\delta_{jk}]/(3N)$.

This stochastic equation has what is known as detailed balance - and hence an exact solution in the steady-state, found by examining the corresponding Fokker-Planck equation:

$$\frac{\partial}{\partial t} P(t, \mathbf{x}) = \mathbf{L}_{FP} P(t, \mathbf{x}) = \sum_i \left[\left(\frac{\partial}{\partial x_i} [\eta + \mathbf{x} \cdot \mathbf{x}/N] x_i + \frac{1}{2} \frac{\partial^2}{\partial x_i^2} \right) P(t, \mathbf{x}) \right] \quad . \quad (16)$$

The equilibrium distribution is $P_e(\mathbf{x}) = \mathcal{N} \exp[-V(\mathbf{x})]$, where $V(\mathbf{x})$ is a potential function given by:

$$V(\mathbf{x}) = \eta \mathbf{x} \cdot \mathbf{x} + (\mathbf{x} \cdot \mathbf{x})^2/2N \quad . \quad (17)$$

The stochastic equation also has an exact relationship between the moments of different orders in the steady-state, which can be easily derived from the variable-change rules of Ito stochastic calculus. These are:

$$\mathcal{M}^{(n+1)} = (2n + N - 2)\mathcal{M}^{(n-1)}/(2N) - \eta\mathcal{M}^{(n)} \quad (18)$$

Here we have defined $\mathcal{M}^{(n)} = \langle [\mathbf{x} \cdot \mathbf{x}]^n \rangle_e/N$, as a convenient normalized form of the moment. Although these recursion relations are useful, the mean-square fluctuations have to be calculated from the potential solutions given above. The quantity $\mathcal{M}^{(1)} = \langle \mathbf{x} \cdot \mathbf{x} \rangle_e/N$ can therefore be computed explicitly and is given by

$$\mathcal{M}^{(1)} = \sqrt{\frac{N}{4}} U\left(\frac{N+1}{2}, \sqrt{N}\eta\right)/U\left(\frac{N-1}{2}, \sqrt{N}\eta\right) \quad , \quad (19)$$

where $U(a, x)$ denote the Whittaker functions [23]. For $\eta = 0$, this expression simplifies to

$$\mathcal{M}^{(1)} = \sqrt{\frac{2}{N}} \Gamma\left(\frac{N+2}{4}\right)/\Gamma\left(\frac{N}{4}\right) \quad . \quad (20)$$

3.2 $N = 1$ case

An important property of this potential in the one-dimensional case of $N = 1$, is that it possesses a potential barrier at $x = 0$, if $\eta < 0$. This means that there is a progression from a stable ‘below-threshold’ region for $\eta > 0$, (where $x = 0$ is the deterministic stable point), to a critical region for $\eta = 0$ characterized by large fluctuations, and then to a bistable region for $\eta < 0$. This is characterized by local stability in the two potential wells at $x = \pm\sqrt{|\eta|}$.

The $N = 1$ case has been well-studied in terms of its eigenvalue spectrum. Any one-dimensional Fokker-Planck equation can be transformed to an equivalent Schroedinger equation problem with imaginary times[12], by introducing a Schroedinger operator. In this case, it has the form:

$$\begin{aligned} \mathbf{L}_S &= \exp[V(\mathbf{x})/2]\mathbf{L}_{FP}\exp[-V(\mathbf{x})/2] \\ &= [2V''(x) - (V'(x))^2]/8 + \frac{1}{2}\frac{\partial^2}{\partial x^2} \\ &= -\frac{1}{2}[x^3 + \eta x]^2 + [\eta + 3x^2]/2 + \frac{1}{2}\frac{\partial^2}{\partial x^2} \quad . \end{aligned} \quad (21)$$

At large positive values of η , the corresponding Schroedinger potential reduces to a harmonic oscillator problem, with quadratic potential. Transforming back to real time, the eigenvalues of the Fokker-Planck operator are of form:

$$\mathbf{L}_{FP}P_n(\mathbf{x}) = -\lambda_n P_n(\mathbf{x}) \quad , \quad (22)$$

where $\lambda_n = n\eta$. Physically this is easy to understand. The equation is dominated by the linear decay rate η , and integer multiples of η will occur through the decay of integer powers of the variable x .

At large negative values of η , the equation is bistable, and there are two principle eigenvalues. A fast equilibration inside each potential well occurs, with an eigenvalue of $\lambda_f = 2|\eta|$ in the limit of large η . A slow decay also occurs through diffusion over the barrier. Ignoring terms in $|\eta|$ of order (1) in the pre-factor, this gives a slow eigenvalue:

$$\ln[\lambda_s] \simeq -\Delta V + \ln[|\eta|] \simeq -\eta^4/2 + \ln[|\eta|]. \quad (23)$$

It is significant for the stochastic diagram method, that this eigenvalue is exponentially small in the limit of large η . Thus, we cannot expect an accurate estimate of the eigenvalue with any technique involving a finite series of terms in η , and any corresponding spectrum in which λ_s is significant will not be able to be estimated with a finite expansion in powers of η .

3.3 Large N case

For $N > 1$, a similar progression from below to above the critical point holds deterministically, except that there is no bistable region. Instead, for $\eta \ll 0$, there is a region characterized by neutral stability in the subset of phase-space where $|\mathbf{x}| \simeq \sqrt{|\eta|N}$. Thus, there is a continuum of possible deterministically stable behaviour. This phenomenon is sometimes called spontaneous symmetry breaking. To show this more clearly, consider the distribution $P_R(R)$, in the variable $R = |\mathbf{x}|^2/N$. This has a steady-state potential of $V_R(R) = N[\eta R + R^2/2 - (1/2 - 1/N) \ln(R)]$. As a result, for increasing N , the distribution in R is peaked more and more strongly near the value $R_\eta = (\sqrt{2 + \eta^2} - \eta)/2$. In fact, due to the increase in phase-space volume as R increases, there is always an outward ‘entropic’ force even when $\eta > 0$. This means that the stochastic equation at large N is not described well by the deterministic stability theory.

In this limit, the radius approaches a fixed value, due to the balance between the outward entropic force due to increasing phase-space volume, and the inward force due to the nonlinearity. Thus, the moments $\mathcal{M}^{(n)}$ all factorise, and are given by:

$$\mathcal{M}^{(n)} = ([\sqrt{2 + \eta^2} - \eta]/2)^n. \quad (24)$$

The recursion relation for moments now simplifies, and it is straightforward to verify that the above solution does satisfy the recursion relation.

Generally, in a stochastic equation, spontaneous symmetry breaking is accompanied by a type of phase-diffusion, or tangential diffusion in a surface of dimension $N - 1$. Hence, the lack of bistability for any N greater than one results in a dynamical behaviour in which diffusion still occurs, but with a reduced dimensionality. These two types of above-threshold behaviour result in different dynamical regimes for the resulting correlation functions and spectra. In both cases, the above threshold dynamics typically involves more than different time-scale. The radial relaxation to a stable point within a potential well

in the R -space equations generally occurs much faster above threshold than the tangential diffusion.

There are corresponding changes in the large- N dynamics, and the physical explanation for this is interesting. In the limit of $N \rightarrow \infty$, the fast radial equilibration takes place in an approximately quadratic potential well at all values of η . It may be noted that the corresponding (Itô) stochastic equation for radial equilibration involves noise in a multiplicative way. In the general case, we find that:

$$\dot{R} = -2\eta R - 2R^2 + 1 + 2\sqrt{\frac{R}{N}}\xi(t) \quad , \quad (25)$$

where $\langle \xi(t)\xi(t') \rangle = \delta(t-t')$. As well as having multiplicative noise, this equation also shows why the stochastic equation trajectories are confined to an increasingly small region in R -space, as N increases. This occurs because the relative size of the noise term in the radial equation decreases as N increases. Thus, radial equilibration takes place with a fast relaxation rate of

$$\lambda_f = 4R_\eta - 2\eta = 2\sqrt{2 + \eta^2} \quad . \quad (26)$$

In the tangential direction, diffusion takes place on a hyper-spherical surface of fixed radius defined by

$$|\mathbf{x}| = \sqrt{NR_\eta} \quad . \quad (27)$$

Suppose we define a coordinate system so the diffusion starts with a radial coordinate of $x_1 = \sqrt{NR_\eta}$ at time $t = 0$. For small times, the other (tangential) coordinates obey the diffusion equation, so that

$$\langle x_j^2 \rangle = t \quad , \quad (28)$$

for $j > 1$. Since the radius is fixed by the radial equation, it follows that this corresponds to angular diffusion. Projecting each angular variable in turn onto a radius vector in a lower dimensional subspace reduces the length of the resulting vector. Finally, in the subspace of one dimension containing the original (starting) vector, we have:

$$\langle x_1(t) \rangle \simeq \sqrt{NR_\eta[1 - t/NR_\eta]^{(N-1)}} \simeq \sqrt{NR_\eta} \exp[-(1 - 1/N)t/2R_\eta] \quad . \quad (29)$$

This corresponds to a much slower tangential relaxation rate of

$$\lambda_s = (1 - 1/N)/(2R_\eta) \quad (30)$$

in the large N limit. We note that this is not exponential in η , unlike the one-dimensional case. Similar behaviour would occur in the case of finite N and large, negative η , which is also dominated by the tangential diffusion caused by spontaneous symmetry breaking. However, for the case of finite N values, the slow eigenvalue must reduce to $\lambda_s = \eta$ in the limit of large enough positive η .

4 N-dimensional stochastic diagrams

The N -dimensional equation clearly has the same structure as the integral equation associated with the simple cubic process considered in the previous section, except for the linear terms which would complicate the diagrams if retained. Instead, we can simply define $y_i(t) = \exp(\eta_i(t-t_0))x_i(t)$, which obeys a stochastic equation without a linear term. This can then be iterated as previously. The iterative solution has the same diagrammatic structure as before. Using an initial estimate for $x_i(t)$ of $x_i^{(0)}(t) = e^{-\eta_i(t-t_0)}v_i$, where the initial value is $\mathbf{v} = \mathbf{x}(\mathbf{t}_0)$, the basic iterative solution is given by:

$$\begin{aligned} x_i^{(n+1)}(t) &= e^{-\eta_i(t-t_0)}x_i(t_0) \\ &+ \int_{t_0}^t dt' e^{-\eta_i(t-t')} [\xi_i(t') - f_{ijkl}x_j^{(n)}(t')x_k^{(n)}(t')x_l^{(n)}(t')] . \end{aligned} \quad (31)$$

It is easily checked that replacing the approximations $\mathbf{x}^{(n)}$, $\mathbf{x}^{(n-1)}$ by \mathbf{x} , leads to an exact integral equation for $\mathbf{x}(t)$.

We can now identify successive iterations with terms in the stochastic diagrams for vector quantities $x_i(t)$, where each vertex includes a term $-f_{ijkl}$, and each directed arrow corresponds to $\int \exp(-\eta_i(t-t')) \dots$. Thus, in evaluating the diagrams, each vector initial condition is replaced by $v_j \exp(-\eta_j(t-t_0))$, and the noise term $w(t)$ is replaced by:

$$w_i(t) = \int_{t_0}^t dt_1 e^{-\eta_i(t-t_1)} \xi_i(t_1) \quad (32)$$

. To order τ^3 , this can be calculated using the diagrams in Fig (3a)-(3d), by making the associations given in Fig (4). Using the diagrams in Fig (3), one can easily derive an expansion for $x_i(t)$ up to order τ^3 . The details of the resulting stochastic integrals are straightforward, but rather lengthy.

These results are given in the Appendix for the rotationally symmetric case. In the symmetric case, it is also clear that $\mathcal{G}_{ij}^{(1)}(\tau) = 0$ if $i \neq j$ and that

$$\begin{aligned} \mathcal{G}^{(1)}(\tau) &\equiv \mathcal{G}_{ii}^{(1)}(\tau) \\ &= \lim_{t_0 \rightarrow \infty} [\langle \mathbf{x}(\tau+t_0) \cdot \mathbf{x}(t_0) \rangle - \langle \mathbf{x}(\tau+t_0) \rangle \cdot \langle \mathbf{x}(t_0+\tau) \rangle] / N . \end{aligned} \quad (33)$$

4.1 N-dimensional two-time correlation function

Averaging the expression for $x_i(t)$ thus obtained over $\xi(t)$'s, expanding the exponential factors and keeping all terms up to order τ^3 , one obtains the result for

the steady-state or equilibrium two-time correlation function. In this expression the two-time correlation is given in terms of the initial one-time moments of the stochastic process. We note that it is not essential, at this stage, to use equilibrium moments. The same general result occurs regardless of the initial condition, even for the case of transient correlations calculated *without* taking the steady-state limit.

We will focus on the symmetric case here, and simplify the following expression (derived in the Appendix), by using the definition of $\mathcal{M}^{(n)} = \langle R^n \rangle_e = \langle [\mathbf{x} \cdot \mathbf{x}/N]^n \rangle_e$, where the subscript e denotes an equilibrium average:

$$\begin{aligned}
\mathcal{G}^{(1)}(\tau) = & \mathcal{M}^{(1)} - \tau \left[\eta \mathcal{M}^{(1)} + \mathcal{M}^{(2)} \right] \\
& + \tau^2 \left[\left(\frac{\eta^2}{2} - \frac{N+2}{2N} \right) \mathcal{M}^{(1)} + 2\eta \mathcal{M}^{(2)} + \frac{3}{2} \mathcal{M}^{(3)} \right] \\
& - \tau^3 \left[\left(\frac{\eta^3}{6} - \eta \left(\frac{5N+10}{6N} \right) \right) \mathcal{M}^{(1)} \right. \\
& \left. + \left(\frac{13\eta^2}{6} - \frac{7N+26}{6N} \right) \mathcal{M}^{(2)} + \frac{9\eta}{2} \mathcal{M}^{(3)} + \frac{5}{2} \mathcal{M}^{(4)} \right] \\
& + O(\tau^4) .
\end{aligned} \tag{34}$$

Next, we can substitute the known equilibrium moments to obtain a final expression for the correlation function in terms of the mean square fluctuation $\mathcal{M}^{(1)} = \langle \mathbf{x} \cdot \mathbf{x}/N \rangle_e$, although still in a power series in τ . Using the previous relations $\mathcal{M}^{(n+1)} = (2n+N-2)\mathcal{M}^{(n-1)}/(2N) - \eta\mathcal{M}^{(n)}$, and defining

$$a = 1/(2\mathcal{M}^{(1)}), \tag{35}$$

one obtains the following power series:

$$\begin{aligned}
\mathcal{G}^{(1)}(\tau) = & \mathcal{M}^{(1)} \left[1 - a\tau + \tau^2 \left(\frac{N+2}{4N} + \frac{1}{2}\eta a \right) \right. \\
& \left. - \tau^3 \left(\frac{N+8}{12N} a + \frac{1}{6}\eta^2 a - \left(\frac{4-N}{12N} \right) \eta \right) + O(\tau^4) \right] ,
\end{aligned} \tag{36}$$

It is convenient to re-express this as:

$$\mathcal{G}^{(1)}(\tau) = \mathcal{M}^{(1)} \left[1 - \sum_{n=1}^3 a_n \tau^n \right] . \tag{37}$$

where:

$$\begin{aligned}
a_1 &= a \\
a_2 &= -(N+2+2N\eta a)/(4N) \\
a_3 &= ((N+8)a + 2N\eta^2 a - (4-N)\eta)/(12N)
\end{aligned} \tag{38}$$

Although the result is still expressed in terms of the correlation function through a , this quantity can be calculated exactly, either by integrating the distribution function numerically, or by using the Whittaker function representation. In the case of $\eta = 0$, this reduces to $a = \sqrt{N/8\Gamma(N/4)/\Gamma((N+2)/4)}$.

4.2 Correlations of polynomials

The diagrammatic expression for $x_i(t)$ in powers of τ and $W(\tau)$ can also be used to calculate the equilibrium correlations for any polynomial functions of $x_i(t)$. Thus, in the case $N = 1$, for the equilibrium correlations for $R = x^2$:

$$\mathcal{G}^{(2)e}(\tau) = \lim_{t_0 \rightarrow \infty} \langle R(\tau + t_0)R(t_0) \rangle - \langle R(\tau + t_0) \rangle \langle R(t_0) \rangle , \quad (39)$$

we obtain

$$\begin{aligned} \mathcal{G}^{(2)e}(\tau) &= [\mathcal{M}^{(2)} - (\mathcal{M}^{(1)})^2] - \tau[2\mathcal{M}^{(1)}] + \tau^2[2 - 2\eta\mathcal{M}^{(1)}] \\ &\quad - \tau^3[8\mathcal{M}^{(1)} + \frac{4}{3}\eta^2\mathcal{M}^{(1)}] + O(\tau^4) . \end{aligned} \quad (40)$$

Here we notice that $\mathcal{M}^{(2)} = 1/2 - \eta\mathcal{M}^{(1)}$, so the pre-factor in the above expression reduces to:

$$[\mathcal{M}^{(2)} - (\mathcal{M}^{(1)})^2] = \mathcal{G}^{(2)}(0) = \frac{2a^2 - 2\eta a - 1}{4a^2} . \quad (41)$$

Just as in the case above, we can write the two-time correlation function down in terms of the individual power series terms, as:

$$\begin{aligned} a_1^{(2)} &= 4a/[2a^2 - 2\eta a - 1] \\ a_2^{(2)} &= -[8a^2 - 4\eta a]/[2a^2 - 2\eta a - 1] \\ a_3^{(2)} &= 4a(4 + 2\eta^2/3)/[2a^2 - 2\eta a - 1] \end{aligned} \quad (42)$$

5 Spectral calculations

The correlation function in the time domain must be extrapolated to long times in order to compute the spectrum, which involves a Fourier transform over all times. The general spectrum for any steady-state correlation function is:

$$S^{(n)}(\omega) = 2\text{Re} \int_0^\infty d\tau \mathcal{G}^{(n)}(\tau) e^{i\omega\tau} . \quad (43)$$

In order to perform the Fourier transform, some extrapolation of the power series is required. In general, for an arbitrary initial condition, this is a difficult operation to perform. However, in the steady state, the un-subtracted correlation function must factorise at long times to the product of the mean values at

initial and final times. This means that the correlation function defined here gives rise to exponential decay at long times.

In fact, for the type of stochastic differential equations considered here, we expect a discrete spectrum with an exponential decay at long times. However, a simple truncation of the power series at a finite order will not lead to an exponential decay, so we cannot just truncate the power series in time to obtain the spectrum. We will consider two different approaches to extrapolation. The first is to simply represent the correlation function with a finite series of exponentially decaying terms, the second is to approximate the logarithm of the correlation function as a rational function.

We assume that our starting point is an arbitrary correlation function \mathcal{G} , expressed as power series up to p -th order in the stochastic diagrams, of form:

$$\mathcal{G}(\tau) = \mathcal{G}(0)[1 - \sum_{n=1}^p a_n \tau^n] \quad . \quad (44)$$

5.1 Simple exponential extrapolation

This technique represents the correlation function as a finite series of decaying exponential terms. The coefficients can then be matched to the known power series in time on a term-by term basis. This method is especially useful when only a small number of eigenvalues dominates the spectrum.

For a power series calculation to order τ^3 , two distinct exponential terms are required. More generally, any correlation function expanded to order $p = 2p' - 1$ is represented using p' effective eigenvalues as:

$$\mathcal{G}(\tau) = \mathcal{G}(0) \sum_{n=1}^{p'} g_n \exp(-\lambda_n \tau) \quad . \quad (45)$$

Here, for simplicity, we impose the restriction that $\sum_{n=1}^{p'} g_n = 1$. It is also obviously necessary that all the effective decay rates are positive. In the third order stochastic diagram case, on matching powers of τ , one obtains:

$$\begin{aligned} g_1 &= \frac{1}{2} - \frac{a_1^3 + 3a_1a_2 + 3a_3}{2\Delta} \\ g_2 &= \frac{1}{2} + \frac{a_1^3 + 3a_1a_2 + 3a_3}{2\Delta} \\ \lambda_1 &= \frac{-\Delta - 3a_3 - a_2a_1}{2a_2 + a_1^2} \\ \lambda_2 &= \frac{\Delta - 3a_3 - a_2a_1}{2a_2 + a_1^2} \end{aligned} \quad (46)$$

where the denominator term Δ is defined by:

$$\Delta = \sqrt{6a_1^3a_3 - 3a_1^2a_2^2 + 18a_1a_2a_3 - 8a_2^3 + 9a_3^2} . \quad (47)$$

5.1.1 Amplitude correlations - N=1 case

For the case of $\mathcal{G}^{(1)}$ at $N = 1$, the dependence of λ_1 and λ_2 on η is displayed in Fig (5a) by the two solid lines, where the upper line corresponds to λ_1 and the lower line to λ_2 . There is a marked transition in this $N = 1$ case, between the non-bistable behaviour for $\eta \gg 0$, where the two time-scales are identical, and the bistable behaviour for $\eta \ll 0$, where one time-scale becomes very long, corresponding to stochastic ‘barrier-hopping’ over the potential barrier in the distribution function at $x = 0$. In this region, the extrapolation technique used here is obviously less reliable, since the relevant eigenvalue is an exponential function of η . One cannot accurately estimate these long-time tails on the correlation function, purely from the short-time information provided by the stochastic diagrams. In fact, there are other techniques based on multiple time-scales, which are more suitable in this above-threshold region.

Nevertheless, the technique does generate the fast eigenvalue ($\lambda_f = 2|\eta|$) correctly for large negative η . For large positive η , the harmonic oscillator predictions are regained. It is interesting to note that the fast eigenvalue in this case is $\lambda_f = 3|\eta|$; this occurs because the symmetry of the problem means that even order eigenvalues are not significant in the dynamics of $G^{(1)}(t)$ at large damping. The slow eigenvalue is not accurately reproduced at large negative η , since this becomes exponentially slow (i.e. should be a straight-line graph). We will show later, by comparisons to numerical simulations, that the critical dynamics are reproduced accurately.

5.1.2 Amplitude correlations - N=4 case

In Fig (5b), the behaviour of the eigenvalues for $\mathcal{G}^{(1)}$ at $N = 4$ is shown in the solid lines. Here we expect the slow eigenvalue to approach $\lambda_s = .375/(R_\eta)$, where $R_\eta = [\sqrt{2 + \eta^2} - \eta]/2$, while the fast eigenvalue should be $\lambda_f = 2\sqrt{2 + \eta^2}$. Since these are strictly large-N limits, we cannot expect these to be found exactly. These approximate results are actually reproduced with surprising precision, especially in the phase-diffusion limit of large negative η . Thus, we find $\lambda_s = .076$ and $\lambda_f = 10.4$ at $\eta = -5$. The approximate predicted values would be $\lambda_s = .074$, and $\lambda_f = 10.6$, with even better agreement at larger values of $|\eta|$. At large positive η , the slow eigenvalue approaches η , and the fast eigenvalue approaches 3η due to the x^3 term in the stochastic equation. This is a result due (as in the $N = 1$ case) to symmetry properties; the intra-well eigenvalue with $\lambda = 2\eta$ does not contribute to this correlation function.

5.1.3 Intensity correlations - N=1 case

Finally, we consider a quadratic correlation function, which we term the intensity correlation. This is the case of $G^{(2)}$ at N=1. These results for the relaxation rates are given in the solid lines of Fig. (5c). Here we see no trace of the exponentially slow eigenvalue. This describes a sign-reversal process which has little or no effect on intensity correlations. Hence, all the observed relaxation rates are caused by the higher-order eigenvalues for intra-well relaxation. Far below threshold, and above threshold, the eigenvalues approach $2|\eta|$ and $4|\eta|$, which are characteristic of intra-well relaxation. Near the critical point of $\eta = 0$, there is strong critical slowing down, with longest time-scales (smallest eigenvalue) being found at $\eta \simeq -1.5$. Although this region is bistable, it gives the slowest relaxation rate of $\lambda_s = 2.35$; going further into the bistable region speeds up the intra-well relaxation.

5.2 Rational logarithmic extrapolation

An alternative ‘generic’ technique, is to approximate the logarithm of the correlation function as a rational function, with a numerator of one order larger than the denominator. This is guaranteed to have an exponential behaviour at large τ . We call this procedure rational logarithmic extrapolation. It can be applied to a power series of any order, as long as it is known that the series gives rise to exponential decay at long times. It is especially useful for complex spectra that may have several eigenvalues - as long as the values are not too different from each other.

For a power series calculation to order τ^3 , a quadratic rational function is required, so that we can approximate the correlation function to the given order as

$$\mathcal{G}(\tau) = \mathcal{G}(0) \left[\exp - \left(\frac{\alpha\tau + \beta\tau^2}{1 + \gamma\tau} \right) \right] \quad . \quad (48)$$

On matching powers of τ with the previous power-series expression, one obtains the following general results:

$$\begin{aligned} \alpha &= a_1 \\ \gamma &= -\frac{2(a_3 + a_1a_2 + a_1^3/3)}{a_1^2 + 2a_2} \\ \beta &= a_1\gamma + a_1^2/2 + a_3 \end{aligned} \quad (49)$$

These can be used to obtain an extrapolated correlation function in any of the cases treated here. However, it is clearly important to ensure that the asymptotic coefficient, β/γ , is positive - otherwise no decay will occur.

5.2.1 Amplitude correlations - N=1 case

In the expression for $G^{(1)}$, the logarithmic expansion gives:

$$\begin{aligned}\gamma &= \frac{4Na^3 - 6N\eta a^2 + 2N\eta^2 a - 2(N-1)a - (4-N)\eta}{3N + 6 + 6N\eta a - 6Na^2} , \\ \frac{\beta}{\gamma} &= a - \frac{(3N + 6 + 6N(\eta a - a^2))^2}{12N(4Na^3 - 6N\eta a^2 + 2N\eta^2 a - 2(N-1)a - (4-N)\eta)} .\end{aligned}\quad (50)$$

The approximate expressions for the equilibrium correlations of $x(t)$ given above are characterized by two time scales - $\lambda_s = \alpha = a$ and $\lambda_l = \beta/\gamma$ which govern the short and long time behaviors respectively. For the case of $\mathcal{G}^{(1)}$ at $N = 1$, the dependence of λ_s and λ_l on η is displayed in Fig (5a) by the two dashed lines. As previously, there is a marked transition in this $N = 1$ case, between the non-bistable behaviour for $\eta \gg 0$ and the bistable behaviour for $\eta \ll 0$. Since the two time-scales here correspond to overall rates at long and short times, and not effective eigenvalues, the distribution of rates is different below threshold - eigenvalues with a low weighting do not contribute very much to the final rate. For this reason, we see no direct evidence for the fast time-scale below threshold, which corresponds to the relaxation of higher order eigenstates.

In the region of long time-scale ‘barrier-hopping’, the extrapolation technique used here is less reliable. One cannot accurately estimate these long-time tails on the correlation function, purely from short-time information. This can be seen most clearly in the way that the slower of the two time-scales goes off the bottom of the logarithmic graph. At this stage, the longest time-scale is negative, indicating that the rational function approximation has broken down, and would predict an infinite or diverging spectrum. Obviously, the extrapolation is severely inaccurate at this point, and cannot be used this far above threshold.

5.2.2 Amplitude correlations - N=4 case

One might expect that the rational approximations used here should improve above threshold as N increases, as the equations are not bistable for large N . This hypothesis proves to be valid, as we show by the use of numerical stochastic techniques in the following sections. However, the improvement can already be seen in Fig (5b). In Fig (5b), which gives $\mathcal{G}^{(1)}$ at $N = 4$, the slowest relaxation times above threshold are slightly too small compared to the exponential method, which indicates that the ratio of relaxation times is still too large for this method to give correct extrapolations, although the situation is much better than in the bistable case with $N = 1$.

5.2.3 Intensity correlations - $N=1$ case

For intrinsically non-bistable quantities like $\mathcal{G}^{(2)}(\tau)$ the problems above do not occur at all, as shown in Fig (5c), which graphs $\mathcal{G}^{(2)}$ at $N = 1$. Here the results of both extrapolation methods give similar behaviour. This is not immediately evident from the graphs, as the rates defined here do not have identical interpretations. In fact, the generic method of rational function extrapolation is actually better than the exponential method in this case. In order to demonstrate this in detail, we must turn to the full spectral calculation, which include both the relaxation rates and the relative weights.

Before turning to the spectral results, we note that the two-time correlation function for the quadratic correlations in the rational approximation have quite a simple form. Extrapolating to large τ using the rational function approximation as above, we obtain

$$\mathcal{G}^{(2)}(\tau) \simeq [\mathcal{M}^{(2)} - [\mathcal{M}^{(1)}]^2] \left[\exp - \left(\frac{a'\tau + b'\tau^2}{1 + c'\tau} \right) \right] , \quad (51)$$

where, using the result $\mathcal{M}^{(2)} = 1/2 - \eta\mathcal{M}^{(1)}$,

$$\begin{aligned} a' &= 4\mathcal{M}^{(1)}/(1 - 2\eta\mathcal{M}^{(1)} - 2[\mathcal{M}^{(1)}]^2) , \\ c' &= \left(\frac{a'^2}{3} + 4 + \frac{2}{3}\eta^2 - \frac{1 - \eta\mathcal{M}^{(1)}}{\mathcal{M}^{(1)}}a' \right) / \left(\frac{1 - \eta\mathcal{M}^{(1)}}{\mathcal{M}^{(1)}} - \frac{a'}{2} \right) \\ \frac{b'}{c'} &= a' - a' \left(\frac{1 - \eta\mathcal{M}^{(1)}}{\mathcal{M}^{(1)}} - \frac{a'}{2} \right)^2 / \left(\frac{a'^2}{3} + 4 + \frac{2}{3}\eta^2 - \frac{1 - \eta\mathcal{M}^{(1)}}{\mathcal{M}^{(1)}}a' \right) \end{aligned} \quad (52)$$

It is interesting to note from Fig(5c), that even for $N = 1$, the x^2 variable is clearly not bistable, and shows no sign of the characteristic long time-scales of bistable variables. Instead, there is a critical slowing-down near $\eta = 0$, with shorter time-scales at all other η values. This also agrees with the exponential extrapolation results.

5.3 Spectral results

Having computed a long-time extrapolation to the two-time correlation function, it is now possible to calculate the spectrum. A simple Lorentzian spectrum is generated by the first order stochastic diagrams. This approximation we shall see is surprisingly close to the correct spectrum even for finite N values, especially at high frequencies. The reason for this is that the middle to high frequency spectral behaviour is mostly due to the change in slope in the two time correlation function near $\tau = 0$, due to the fact that the steady state correlation function must be a function of $|\tau|$. The low frequency spectral behaviour near $\omega = 0$ has additional contributions due to the $\tau \rightarrow \infty$ behaviour of the

correlation function, which is not always given accurately using a first order expansion in τ . The lowest order spectral contribution is therefore

$$S^{(1)}(\omega) = 2\mathcal{G}^{(1)}(0)Re \int_0^\infty d\tau e^{-a|\tau|+i\omega\tau} = \frac{1}{a^2 + \omega^2} \quad , \quad (53)$$

where $a = 1/[2\langle R \rangle]$ is defined as in the previous sections. Thus, in the large N limit we expect to find that:

$$\lim_{N \rightarrow \infty} S^{(1)}(\omega) = \frac{4R_\eta^2}{(1 + (2R_\eta\omega)^2)^2} \quad . \quad (54)$$

To higher order, it is necessary to choose which extrapolation method to use. The procedure of extrapolating the correlation function to large τ by expanding it as a series of exponentially decaying terms, is simple to Fourier transform, since this clearly results in:

$$\mathcal{S}(\omega) = \mathcal{G}(0) \sum_{n=1}^{p'} \frac{2g_n\lambda_n}{\lambda_n^2 + \omega^2} \quad . \quad (55)$$

This results in a Fourier transform as a sum of Lorentzian components. For the three previous cases treated of $N = 1$, $N = 4$, and the intensity spectrum for $N = 1$, the spectrum thus obtained is plotted in Fig (6a) -(6c) for various values of η . The clear progression from bistable behaviour, to spontaneous symmetry-breaking, to non-bistable behaviour, is shown in these three graphs; as the peak spectral intensity is greatly reduced for the spectra with shorter characteristic time-scales.

While this procedure has advantages as far as calculating the Fourier transform is concerned, it is not always the best extrapolation. Accordingly, we also consider a straightforward numerical Fourier transform, which can be used to calculate the spectrum from the rational function approximation to the correlation functions.

5.4 Direct numerical simulation

As there are no exactly known analytic expressions for these spectra, we have to resort to stochastic numerical techniques to check the accuracy of the spectrum using the truncated diagram method. Thus, in order to determine the accuracy of the correlation function, a direct simulation of the relevant stochastic differential equations was used. These simulations employed a strongly convergent semi-implicit numerical algorithm [24], with checks on both numerical sampling error and truncation error due to finite step-size. The actual algorithm used employed four iterations of the nonlinear implicit equations at each step. After starting the trajectories in a Gaussian distribution with variance equal to the

known steady state variance, each trajectory was integrated for a total elapsed time much longer than the correlation time.

Typically, $t = 100 - 400$ was the maximum time used, with longer times being employed for calculations above threshold, where the correlation time is longer. In the simulations, the total number of trajectories employed was 10^6 , in order to reduce the sampling error to typically about $0.1 - 0.2\%$ at low frequencies - although this typically rose to about 0.5% above threshold, presumably because of the highly non-Gaussian individual trajectory statistics in these cases. Sampling errors were checked by subdividing the results into 1000 sub-ensembles, which were numerically Fourier transformed and averaged individually. The spectral results were then averaged over the sub-ensembles, and the error-bar in the overall mean was estimated using standard Gaussian distribution error estimates – on the basis that sub-ensemble means should have a Gaussian distribution according to the central limit theorem.

By reducing the time step to a small value (typically $\Delta t = 0.01 - 0.05$), the errors due to the finite step-size were typically kept to below 0.5% . This was estimated by calculating all spectra at two different step-sizes, but with the same underlying stochastic noise terms, and comparing the results. The two error-bars were added to give the final numerical error-estimates. No significant error from finite spectral windowing was found, although this would be expected to give problems in the extreme bistable regions.

By comparing with exact zero-frequency results, this technique of error-estimation proved a reliable method, in the sense that the discrepancies were of the expected size.

Thus, for example, the numerical spectrum for the case of $N = 1$ at threshold ($\eta = 0$) has the calculated value of $S(0) = 0.966 \pm 0.007$, using 10^6 trajectories, a window of $t_{MAX} = 200$, and a step-size of $\Delta t = 0.025$. The error due to the finite step-size contributes ± 0.005 to the total error. The corresponding exact result, as explained in the next section, is $S(0) = 0.975$ - giving a slightly greater actual numerical error than the estimated one standard-deviation error-bar. By comparison, the extrapolated exponential series analytic result is $S(0) = 0.970$, which is very close to the exact result.

For the case of $N = 1$ above threshold ($\eta = -1.5$) the calculated numerical simulation value is $S(0) = 10.01 \pm 0.10$, using 10^6 trajectories, a window of $t_{MAX} = 400$, and a step-size of $\Delta t = 0.05$. Because the step-size is relatively large (in order to maximize the time-window), the error-bar in this case is mostly due to the finite step-size, which contributes an error of ± 0.08 to the total error. The corresponding exact result is $S(0) = 10.11$ - within the estimated error-bars. By comparison, the extrapolated analytic result is $S(0) = 9.06$, which gives an increased extrapolation error, as expected.

The resulting numerical estimate of $S^{(n)}(\omega)$ was:

$$S_{num}^{(n)}(\omega) = \lim_{T \rightarrow \infty} \langle |\widetilde{\Delta x_i^n}(\omega)|^2 \rangle / T , \quad (56)$$

where the Fourier transform $\Delta\widetilde{x_i^n}(\omega)$ is defined as

$$\Delta\widetilde{x_i^n}(\omega) = \int_0^T dt e^{i\omega t} [x_i^n(t) - \langle x_i^n(t) \rangle] \quad . \quad (57)$$

5.5 Comparison of results

The results of the two procedures, i.e. stochastic diagrams and numerical simulations, are compared in Figs (7), (8) and (9) for $N = 1$, $N = 4$ and the intensity spectrum with $N = 1$ respectively. In each figure there are four lines, which are the Lorentzian approximation (dotted line), the rational approximation (dashed-dotted line), the second order exponential series extrapolation (dashed line) and the direct numerical simulations (solid line).

In each figure there are sub-figures which correspond to different values of the driving field η , which are taken through a range of values from far below threshold to above threshold. We notice that agreement is generally excellent (close to the simulation error-bars) for all methods below threshold. Errors are always worst at low frequencies, where the results are the most sensitive to the extrapolation error at long times. They are also worst for the single exponential extrapolation than the higher-order extrapolation methods, as expected, and usually best for the exponential series method.

5.5.1 Amplitude correlations - $N=1$ case

Below threshold, Fig (7a) shows the four different spectral results near zero-frequency, thus giving a magnified view of the results. Errors are much smaller at higher frequencies, where all the techniques agree to within the simulation error-bars. It can be seen that the exponential series method (dashed line) gives the best low-frequency agreement to the simulation (solid line). The residual difference is about equal to the intrinsic numerical discretization and sampling errors, while the other two methods give small, but marginally significant discrepancies.

In Fig (7b), at the critical point of $\eta = 0$, the exponential series gives a prediction at $N = 1$ of $S(0) = 0.9702$. This is in quite remarkable agreement with the simulated value of $S(0) = 0.966 \pm 0.007$. By comparison, the other two methods are again either significantly higher (rational logarithmic), or lower (Lorentzian approximation).

Above threshold, however, in Fig (7c), we see that the agreement is outside the error-bars even for the exponential series method, thus indicating a reduced accuracy in the long-time extrapolation. This is expected, in view of the fact that the long-time eigenvalue is an exponential function of η - rather than a finite algebraic expression, as would be generated from the stochastic diagrams. Here the errors increase to about 15% for $\eta = -1.5$, at zero frequency, in the rational approximation, with much worse errors in the single exponential approximation.

However, in this case the exponential series still gives the best result, with an error of less than 10% .

5.5.2 Amplitude correlations - N=4 case

Fig (8) shows the spectrum of $x(t)$ as a function of η at $N = 4$. In Fig (8a), with $\eta = 1$ (below threshold) the difference between the various approximations and the numerical simulation is about equal to the sampling error-bars obtained with 10^6 trajectories. Thus, it is not possible to distinguish between any of the extrapolations in this case. At threshold, in Fig (8b), the differences increase, and the exponential series method is clearly better than a single exponential extrapolation. Above threshold, in Fig (8c), the accuracy of both the single exponential and the rational extrapolation diminishes, relative to the exponential series method - due to the two dominant eigenvalues in this case. For $N = 4$, the above threshold error with the rational extrapolation reduced to 7%, as the multiple time-scale problem is less significant in this case. The error in the exponential series method is less than 1%, i.e., of the same order as the intrinsic sampling errors.

5.5.3 Intensity spectrum - N=1 case

Fig (9) shows the spectrum of $x^2(t)$ as a function of η as given by the different approximations. We see that there are obvious differences between this and the previous cases. As $x^2(t)$ is not bistable, the spectrum does not have a large ‘spike’ as $\eta \rightarrow -\infty$. This means that, unlike the previous examples, the agreement between the rational function extrapolation and simulation methods remains of the order of the numerical sampling error-bars even above threshold. Since it would presumably require more than 10^6 trajectories to resolve the differences in these spectral results, we have not attempted to accurately estimate the extrapolation errors here. For this problem, it is clear that the analytical theory is rather competitive with numerical simulations, which are always subject to numerical sampling error. The nearly perfect agreement for rational function extrapolation is a surprising result, given that it is obtained from only a small number of stochastic diagrams. In this case, the exponential series method gives slightly worse results, presumably because there are several competing eigenvalues rather than just two.

5.6 Exact results

Although the agreement between the analytic results and the numerical simulations is generally excellent (except for bistable variables) there are some features worth a closer examination. Firstly, we emphasize again that discrepancies are only evident at low frequencies. This is simply because the correlation function tails, although only contributing a small part of the spectrum, cannot always

be accurately extrapolated from the short time power series expansion. This discrepancy at or below the critical point is always small (of order of 1 – 2% at the critical point $\eta = 0$). The error is naturally larger in the simpler Lorentzian approximation, but in no case does it exceed 5% with $\eta = 0$. Secondly, the low frequency extrapolation error is larger above threshold as $\eta \rightarrow -\infty$, especially in the bistable case of $x(t)$ spectrum with $N = 1$. This result is expected, since calculation of the slow eigenvalue in this case requires an infinite series in η .

In the particular case of $N = 1$, the zero frequency spectrum is known exactly [7] and is given by

$$S^{(n)}(0) = 4 \int_{-\infty}^{\infty} dx \frac{[f^{(n)}(x)]^2}{P_{eq}(x)} \quad , \quad (58)$$

where

$$f^{(n)}(x) = - \int_{-\infty}^x dx_1 [x_1^n - \langle x^n \rangle] P_{eq}(x_1) \quad . \quad (59)$$

Here $P_{eq}(x)$ denotes the normalized equilibrium distribution. The discrepancy between this exact result at $N = 1$, and the approximate spectra, is given in Fig (10).

In the bistable case of $S^{(1)}$, it is clear that the error increases very rapidly as $\eta \rightarrow -\infty$, especially for the single exponential and rational approximations. The reason for this is due to the well known bifurcation of the deterministic steady state in this case, when $\eta \ll 0$. The system can only switch from one solution near $x = \eta$ to the other near $x = -\eta$, on exponentially long time scales. This can be seen on comparing Fig (11), which is computed at the deterministic threshold of $\eta = 0$, with an above threshold numerical simulation in Fig (12). In this region and above, a multiple time scale technique would give the best results, with other methods being used to estimate the slow eigenvalue. As we are interested here in the critical region around $\eta = 0$, we simply note this problem here, rather than pursuing it in further detail. Techniques for dealing with multiple time-scales of these barrier-hopping equations were first developed by Kramers[25], and are quite well understood.

This type of problem is greatly reduced for $N > 1$, where there is a tangential diffusion above threshold, rather than barrier-hopping. This results in an increasing accuracy of the present technique for large N , as the system dynamics reduces to just two time-scales, both of which have finite expression in terms of η . In this limit, the behaviour is closely analogous to the well-known problem of diffusion in a curved space. While there are no examples of physical systems with such large-dimensional order-parameters, many physical systems (like the laser above threshold, or Bose-Einstein condensates) display this type of spontaneous symmetry breaking accompanied by tangential diffusion in phase-space. The case chosen ($N = 4$) is typified by a two mode laser with inhomogeneous broadening, so there is no strong mode-competition. As we have seen, the stochastic diagram method gives very accurate results when

compared with numerical simulations. However, we have no exact result in this case.

Multiple time-scale problems do not occur in the case of non-bistable quantities like $x^2(t)$ whose spectrum is given in Fig. (10b). The exponential series method gives good agreement, as expected. Agreement with the rational function extrapolation in this case is excellent even above threshold. It is so good that the exact spectral result at $\omega = 0$ cannot be told apart from the approximate value, so we have not included the rational approximation in this graph.

6 Summary

The stochastic diagram technique is a method of classifying iterative terms in a stochastic power series expansion in time, so that terms of the same order in time are grouped together. This involves analyzing the deterministic and stochastic order, since they give rise to different types of contributions.

In this paper we have used this technique to analyze critical amplitude and intensity spectra, by considering either exponential series or logarithmic rational function extrapolation. The results are inherently non-perturbative, and are very accurate except in bistable regions. Thus, the results are valid at the critical point, where linearized spectra diverge. Good results are also obtained even above threshold using exponential series extrapolation, when there is spontaneous symmetry-breaking. The technique works especially well for intrinsically non-bistable quantities like the intensity or radial spectrum. In these cases, we find that rational function extrapolation is of greater accuracy.

The general feature of these results for the case of the cubic stochastic process, is that we see the expected critical slowing down at the threshold or critical point at $\eta = 0$. Below threshold, there is rather stable behaviour, except at high dimensionality where the outward entropic effects of the phase-space volume are increasingly important. Above threshold, there is a bistable region for $N = 1$, where our methods do not converge quickly, due to the exponentially long time-scales involved. For this region, asymptotic methods involving multiple time-scales would be more suitable. For $N > 1$, our method gives much better results than for $N = 1$ above threshold, since the dynamics in this region are then dominated by a type of phase-diffusion at fixed radius, rather than by barrier-hopping.

The problems treated here were of a relatively simple type, to allow comparisons with exactly known results. We emphasize that the stochastic diagram approach is rather general. It is not restricted to equilibrium correlations, although extrapolation is not always possible in transient calculations. Nor is it restricted to problems just involving temporal variation: partial stochastic differential equations can also be treated in this way.

In summary, this novel stochastic diagram technique appears to have many possible applications for calculations involving stochastic differential equations.

One of us (SC) is grateful to the University of Queensland for the University of Queensland Travel Award for International Collaborative Research which made this work possible.

Appendix

In this appendix we briefly outline the details of the calculations leading to the result given in (34), using the rules given in Fig (4).

The contributions to the diagrams in Fig (3a) can easily be written down as follows

$$\begin{aligned}\tilde{x}_i^{(0)}(t) &= e^{-\eta t} v_i \\ \tilde{x}_i^{(1/2)}(t) &= w_i(t)\end{aligned}\quad (1)$$

Next, evaluating the diagrams with one vertex in Fig (3b), gives:

$$\begin{aligned}\tilde{x}_i^{(1)}(t) &= -f_{ijkl} \int_0^t dt_1 e^{-\eta(t+2t_1)} v_j v_k v_l \\ \tilde{x}_i^{(3/2)}(t) &= -3f_{ijkl} \int_0^t dt_1 e^{-\eta(t+t_1)} w_j(t_1) v_k v_l\end{aligned}\quad (2)$$

The next order terms in Fig (3c) include both one-vertex terms with additional noise factors, and two-vertex nested integral terms:

$$\begin{aligned}\tilde{x}_i^{(2)}(t) &= 3f_{ijkl} \left[- \int_0^t dt_1 e^{-\eta t} w_j(t_1) w_k(t_1) v_l \right. \\ &\quad \left. + f_{lmnp} \int_0^t dt_1 e^{-\eta(t+2t_1)} v_j v_k \int_0^{t_1} dt_2 e^{-2\eta t_2} v_m v_n v_p \right] \\ \tilde{x}_i^{(5/2)}(t) &= 3f_{ijkl} \left[- \int_0^t dt_1 e^{-\eta(t-t_1)} w_j(t_1) w_k(t_1) w_l(t_1) \right. \\ &\quad \left. + 3f_{lmnp} \int_0^t dt_1 e^{-\eta(t+2t_1)} v_j v_k \int_0^{t_1} dt_2 w_m(t_2) e^{-\eta t_2} v_n v_p \right. \\ &\quad \left. + 2f_{lmnp} \int_0^t dt_1 e^{-\eta(t+t_1)} v_j w_k(t_1) \int_0^{t_1} dt_3 e^{-2\eta t_3} v_m v_n v_p \right]\end{aligned}\quad (3)$$

Finally, the relevant third order terms are:

$$\begin{aligned}\tilde{x}_i^{(3)}(t) &= 3f_{ijkl} e^{-\eta t} \left[f_{lmnp} \int_0^t dt_1 w_j(t_1) w_k(t_1) \int_0^{t_1} dt_2 e^{-2\eta t_2} v_m v_n v_p \right. \\ &\quad \left. + 3f_{lmnp} \int_0^t dt_1 e^{-2\eta t_1} v_j v_k \int_0^{t_1} dt_2 w_m(t_2) w_n(t_2) v_p \right]\end{aligned}$$

$$\begin{aligned}
& + 6f_{lmnp} \int_0^t dt_1 e^{-\eta t_1} v_j w_k(t_1) \int_0^{t_1} dt_2 e^{-\eta t_2} w_m(t_2) v_n v_p \\
& - f_{kmnp} f_{lqrs} \int_0^t dt_1 e^{-2\eta t_1} v_j \int_0^{t_1} dt_2 e^{-2\eta t_2} v_m v_n v_p \int_0^{t_1} dt_3 e^{-2\eta t_3} v_q v_r v_s \\
& - 3f_{lmnp} f_{pqrs} \int_0^t dt_1 v_j v_k \int_0^{t_1} dt_2 v_m v_n \int_0^{t_2} dt_3 e^{-2\eta(t_1+t_2+t_3)} v_q v_r v_s \Big] . \tag{4}
\end{aligned}$$

In the above equations summation over repeated indices is implied. The next step consists in

- (a) multiplying the above expressions by $v_i = x_i(0)$ and summing over i
- (b) averaging the resulting expressions over the noise sources and the initial values and adding up all the contributions.

This leads to

$$\begin{aligned}
\frac{\langle \mathbf{x}(t) \cdot \mathbf{x}(0) \rangle}{N} & = e^{-\eta t} \frac{1}{N} \langle \mathbf{v} \cdot \mathbf{v} \rangle - \frac{1}{N} f_{ijkl} \langle v_i v_j v_k v_l \rangle \int_0^t dt_1 e^{-\eta(t+2t_1)} \\
& + \frac{3e^{-\eta t} f_{ijkl}}{N} \left[-\delta_{jk} \langle v_i v_l \rangle \int_0^t dt_1 \int_0^{t_1} dt_2 e^{-2\eta(t_1-t_2)} \right. \\
& + f_{lmnp} \langle v_i v_j v_k v_m v_n v_p \rangle \int_0^t dt_1 \int_0^{t_1} dt_2 e^{-2\eta(t_1+t_2)} \\
& + f_{lmnp} \delta_{jk} \langle v_i v_m v_n v_p \rangle \int_0^t dt_1 \int_0^{t_1} dt_2 \int_0^{t_1} dt_3 e^{-2\eta(t_1-t_2+t_3)} \\
& + 3f_{lmnp} \delta_{mn} \langle v_i v_j v_k v_p \rangle \int_0^t dt_1 \int_0^{t_1} dt_2 \int_0^{t_2} dt_3 e^{-2\eta(t_1+t_2-t_3)} \\
& + 6f_{lmnp} \delta_{km} \langle v_i v_j v_n v_p \rangle \int_0^t dt_1 \int_0^{t_1} dt_3 \int_0^{t_3} dt_2 e^{-\eta(t_1-t_2)} \\
& - f_{kmnp} f_{lqrs} \langle v_i v_j v_m v_n v_p v_q v_r v_s \rangle \int_0^t dt_1 \left(\int_0^{t_1} dt_2 e^{-\eta(t_1+2t_2)} \right)^2 \\
& - 3f_{lmnp} f_{pqrs} \langle v_i v_j v_k v_m v_n v_q v_r v_s \rangle \\
& \times \left. \int_0^t dt_1 \int_0^{t_1} dt_2 \int_0^{t_2} dt_3 e^{-2\eta(t_1+t_2+t_3)} \right] . \tag{5}
\end{aligned}$$

For the symmetric case with f_{ijkl} given by $f_{ijkl} = [\delta_{ij}\delta_{kl} + \delta_{ik}\delta_{jl} + \delta_{il}\delta_{jk}]/(3N)$, the above results can be simplified. This is not essential to the method, and neither is the use of a steady-state initial condition at this stage. On explicitly carrying out the summations, we obtain

$$\frac{\langle \mathbf{x}(t) \cdot \mathbf{x}(0) \rangle}{N} = \frac{e^{-\eta t}}{N} \left[\langle \mathbf{v} \cdot \mathbf{v} \rangle - \frac{1}{N} \langle (\mathbf{v} \cdot \mathbf{v})^2 \rangle \int_0^t dt_1 e^{-2\eta t_1} \right]$$

$$\begin{aligned}
& -\frac{(N+2)}{N} \langle \mathbf{v} \cdot \mathbf{v} \rangle \int_0^t dt_1 \int_0^{t_1} dt_2 e^{-2\eta(t_1-t_2)} \\
& + \frac{3}{N^2} \langle (\mathbf{v} \cdot \mathbf{v})^3 \rangle \int_0^t dt_1 \int_0^{t_1} dt_2 e^{-2\eta(t_1+t_2)} \\
& + \frac{(N+2)}{N^2} \langle (\mathbf{v} \cdot \mathbf{v})^2 \rangle \int_0^t dt_1 \int_0^{t_1} dt_2 \int_0^{t_1} dt_3 e^{-2\eta(t_1-t_2+t_3)} \\
& + \frac{3(N+2)}{N^2} \langle (\mathbf{v} \cdot \mathbf{v})^2 \rangle \int_0^t dt_1 \int_0^{t_1} dt_2 \int_0^{t_2} dt_3 e^{-2\eta(t_1+t_2-t_3)} \\
& + \frac{2(N+8)}{N^2} \langle (\mathbf{v} \cdot \mathbf{v})^2 \rangle \int_0^t dt_1 \int_0^{t_1} dt_3 \int_0^{t_3} dt_2 e^{-\eta(t_1-t_2)} \\
& - \frac{3}{N^3} \langle (\mathbf{v} \cdot \mathbf{v})^4 \rangle \int_0^t dt_1 \left(\int_0^{t_1} dt_2 e^{-\eta(t_1+2t_2)} \right)^2 \\
& - \frac{9}{N^3} \langle (\mathbf{v} \cdot \mathbf{v})^4 \rangle \int_0^t dt_1 \int_0^{t_1} dt_2 \int_0^{t_2} dt_3 e^{-2\eta(t_1+t_2+t_3)}. \quad (6)
\end{aligned}$$

Finally, replacing the initial averages by equilibrium averages and expanding the time integrals in powers of t we obtain

$$\begin{aligned}
\frac{\langle \mathbf{x}(t) \cdot \mathbf{x}(0) \rangle}{N} &= \mathcal{M}^{(1)} \left[1 - \eta t + \frac{1}{2} \eta^2 t^2 - \frac{1}{6} \eta^3 t^3 + \dots \right] \\
&- \mathcal{M}^{(2)} \left[t - 2\eta t^2 + \frac{13}{6} \eta^2 t^3 + \dots \right] \\
&- \frac{(N+2)}{N} \mathcal{M}^{(1)} \left[\frac{1}{2} t^2 - \frac{5}{6} \eta t^3 + \dots \right] \\
&+ 3\mathcal{M}^{(3)} \left[\frac{1}{2} t^2 - \frac{3}{2} \eta t^3 + \dots \right] \\
&+ \frac{(N+2)}{N} \mathcal{M}^{(2)} \left[\frac{5}{6} t^3 + \dots \right] + \frac{2(N+8)}{N} \mathcal{M}^{(2)} \left[\frac{1}{6} t^3 + \dots \right] \\
&- \mathcal{M}^{(4)} \left[\frac{5}{2} t^3 + \dots \right]. \quad (7)
\end{aligned}$$

On collecting coefficients of like powers of t we are led to the expression (34) for the short time expansion of the two-time correlation function in the N -dimensional case with rotational symmetry. This also agrees with the earlier result of Eq (12), for the simpler case of $N = 1$ and $\eta = 0$ – as expected.

References

- [1] P. Langevin, Comptes. Rendues **146**, 530 (1908).
- [2] A. Einstein, Ann. Phys. (Leipzig) **21**, 756 (1906).

- [3] K. Ito, Nagoya Mathematics Journal **3**, 55 (1951).
- [4] R. L. Stratonovich, SIAM Journal on Control **4**, 362 (1966).
- [5] H. Haken, *Synergetics: An introduction*, (Springer Verlag, Berlin, Heidelberg, New York; 1978).
- [6] M. F. M. Osborne, Operations Research **7**, 145 (1959); F. Black and M. Scholes, Journal of Political Economy **81**, 637 (1973); Clifford W. Smith, Jr., Journal of Financial Economics **3**, 3 (1976).
- [7] M. Tehrani and L. Mandel, Phys. Rev. A **17**, 677 (1978).
- [8] F. T. Hioe, Surendra Singh and L. Mandel, Phys. Rev. A **19**, 2036 (1979).
- [9] Surendra Singh and L. Mandel, Phys. Rev. A **20**, 2459 (1979).
- [10] P. D. Drummond and P. Kinsler, Quantum and Semiclass. Opt **7**, 727 (1995).
- [11] P. D. Drummond and P. Kinsler, Phys. Rev. A **52**, 783 (1995).
- [12] H. Risken, *The Fokker-Planck Equation*, (Springer Verlag, Berlin, Heidelberg, New York; 1989).
- [13] P. Jung and H. Risken, Z. Physik B **59**, 469 (1985).
- [14] W. Nadler and K. Schulten, Z. Physik B **59**, 53 (1985) ; Z. Physik B **72**, 53 (1987).
- [15] M. San Miguel, L. Pesquera, M. A. Rodriguez and A. Hernández-Machado, Phys. Rev. A **35**, 208 (1987).
- [16] N. G. van Kampen, J. Stat. Phys. **17**, 71 (1977).
- [17] H. Dekker and N. G. van Kampen, Phys. Lett. A **73**, 374 (1979).
- [18] R. Zwanzig, in *Lectures in Theoretical Physics* eds W. Brittin and L. Dunham, Vol 3, (Wiley, New York; 1961).
- [19] H. Mori, Prog. Theor. Phys. **34**, 399 (1965).
- [20] S. K. Ma, *Modern Theory of Critical Phenomena*, (W.A. Benjamin, Reading, Mass.; 1976).
- [21] S. Chaturvedi, A. K. Kapoor and V. Srinivasan, *Stochastic Quantization of Parisi and Wu*, (Bibliopolis, Naples; 1990).
- [22] C. W. Gardiner, *Handbook of Stochastic Methods*, (Springer Verlag, Berlin, Heidelberg, New York; 1985).

- [23] M. Abramowitz and I. A. Stegun, *Handbook of Mathematical Functions*, (Dover, New York; 1965).
- [24] P. D. Drummond and I. K. Mortimer, J. Comp. Phys. **93**, 144 (1991).
- [25] H. A. Kramers, Physica **7**, 284 (1940).

Figure 1: Diagrammatic representation of the iterative solution of the cubic stochastic equation to zeroth and first order.

Figure 2: Diagrammatic representation of the iterative solution of the cubic stochastic equation to second order.

Figure 3: Diagrammatic representation of the iterative solution of the cubic stochastic equation reordered by collecting together the diagrams which contribute to the same power of τ . The power of τ that each diagram contributes, is equal to the number of vertices plus half the number of crosses. Figs (a) - (d) indicate successively higher order diagrams, including fractional stochastic orders.

Figure 4: The rules for writing down the contribution of a given diagram.

Figure 5: The dependence of the apparent relaxation rates on the loss rate η as given by the exponential series (solid line) and rational function (dotted line) extrapolations. Note that the two types of extrapolation implicitly define different types of relaxation rate. In each graph, the lower of the two lines corresponds to the slower relaxation rate, the upper to the faster relaxation rate. Cases treated are for (a) $G^{(1)}$, $N = 1$; (b) $G^{(1)}$, $N = 4$; (c) $G^{(2)}$, $N = 1$.

Figure 6: The approximate equilibrium spectrum for range of values of η , using the exponential series method. Cases treated are for (a) $S^{(1)}(\omega)$, $N = 1$; (b) $S^{(1)}(\omega)$, $N = 4$; (c) $S^{(2)}(\omega)$, $N = 1$.

Figure 7: Comparison of the equilibrium spectrum $S^{(1)}(\omega)$ of $x(t)$ for $N = 1$ as given by stochastic numerical simulations (solid line), exponential series extrapolation (dashed line), rational function extrapolation (dashed-dotted line), Lorentzian approximation (dotted line) for (a) $\eta = 1$, (b) $\eta = 0$, (c) $\eta = -1.5$. Error-bars for discretization and sampling errors at zero frequency are: (a) $\Delta S = 0.002$, (b) $\Delta S = 0.007$, (c) $\Delta S = 0.1$.

Figure 8: Comparison of the equilibrium spectrum $S^{(1)}(\omega)$ of $x(t)$ for $N = 4$ as given by stochastic numerical simulations (solid line), exponential series extrapolation (dashed line), rational function extrapolation (dashed-dotted line), Lorentzian approximation (dotted line) for (a) $\eta = 1$, (b) $\eta = 0$, (c) $\eta = -1.5$. Sampling error-bars at zero frequency are: (a) $\Delta S = 0.002$, (b) $\Delta S = 0.01$, (c) $\Delta S = 0.1$.

Figure 9: Comparison of the equilibrium spectrum $S^{(2)}(\omega)$ of $x^2(t)$ for $N = 1$ as given by exact numerical simulations (solid line), exponential series extrapolation (dashed line), rational function extrapolation (dashed-dotted line), Lorentzian approximation (dotted line) for (a) $\eta = 1$, (b) $\eta = 0$, (c) $\eta = -1.5$. Sampling error-bars at zero frequency are: (a) $\Delta S^{(2)} = 0.0003$, (b) $\Delta S^{(2)} = 0.001$, (c) $\Delta S^{(2)} = 0.004$.

Figure 10: Comparison of the equilibrium spectrum for $N = 1$ at zero frequency as given by the exact analytic expression (solid line), exponential series extrapolation (dashed line), rational function extrapolation (dashed-dotted line), Lorentzian approximation (dotted line) for a range of values of η . Cases treated are: (a) $S^{(1)}(0)$; (b) $S^{(2)}(0)$.

Figure 11: A sample numerical run showing critical fluctuations of $x(t)$ at threshold, for the case $\eta = 0$, $N = 1$.

Figure 12: A sample numerical run showing bistability of $x(t)$ above threshold, for the case $\eta = -1.5$, $N = 1$.

$$X^{(0)}(t) = \rightarrow$$

$$X^{(1)}(t) = \rightarrow + \rightarrow \times + \text{dot product diagram}$$

Fig. 1

$$X^{(2)}(t) = \text{Diagram 1} + \text{Diagram 2} + \text{Diagram 3} + \text{Diagram 4} + 3 \text{Diagram 5} + 3 \text{Diagram 6} + 6 \text{Diagram 7} + 3 \text{Diagram 8} + 3 \text{Diagram 9} + 3 \text{Diagram 10} + 3 \text{Diagram 11}$$

Diagram 1: A horizontal line with an arrow pointing right. A small circle with an 'x' is placed on the line.

Diagram 2: A horizontal line with an arrow pointing right. A small circle with an 'x' is placed on the line.

Diagram 3: A horizontal line with an arrow pointing right. A small circle with an 'x' is placed on the line.

Diagram 4: A horizontal line with an arrow pointing right. A small circle with an 'x' is placed on the line.

Diagram 5: A horizontal line with an arrow pointing right. A small circle with an 'x' is placed on the line.

Diagram 6: A horizontal line with an arrow pointing right. A small circle with an 'x' is placed on the line.

Diagram 7: A horizontal line with an arrow pointing right. A small circle with an 'x' is placed on the line.

Diagram 8: A horizontal line with an arrow pointing right. A small circle with an 'x' is placed on the line.

Diagram 9: A horizontal line with an arrow pointing right. A small circle with an 'x' is placed on the line.

Diagram 10: A horizontal line with an arrow pointing right. A small circle with an 'x' is placed on the line.

Diagram 11: A horizontal line with an arrow pointing right. A small circle with an 'x' is placed on the line.

Fig. 2

$$\tilde{X}^{(0)}(t) = \rightarrow$$

$$\tilde{X}^{(1/2)}(t) = \rightarrow \times$$

Fig. 3a

$$\tilde{X}^{(1)}(t) = \begin{array}{c} \uparrow \\ \rightarrow \\ \leftarrow \\ \downarrow \end{array}$$

$$\tilde{X}^{(3/2)}(t) = 3 \begin{array}{c} \uparrow \\ \rightarrow \\ \leftarrow \\ \downarrow \end{array}$$

Fig. 3b

$$\tilde{X}^{(2)}(t) = 3 \begin{array}{c} \text{Diagram:} \\ \text{Two nodes connected by a horizontal line.} \\ \text{Top node: Up, Left, Right} \\ \text{Bottom node: Down, Left, Right} \\ \text{Crosses at the center} \end{array} + 3 \begin{array}{c} \text{Diagram:} \\ \text{Two nodes connected by a horizontal line.} \\ \text{Top node: Up, Left, Right} \\ \text{Bottom node: Up, Left, Right} \\ \text{Crosses at the center} \end{array}$$

$$\tilde{X}^{(5/2)}(t) = \begin{array}{c} \text{Diagram:} \\ \text{Two nodes connected by a horizontal line.} \\ \text{Top node: Up, Left, Right} \\ \text{Bottom node: Down, Left, Right} \\ \text{Crosses at the center} \end{array} + 9 \begin{array}{c} \text{Diagram:} \\ \text{Two nodes connected by a horizontal line.} \\ \text{Top node: Up, Left, Right} \\ \text{Bottom node: Up, Left, Right} \\ \text{Crosses at the center} \end{array} + 6 \begin{array}{c} \text{Diagram:} \\ \text{Two nodes connected by a horizontal line.} \\ \text{Top node: Up, Left, Right} \\ \text{Bottom node: Up, Left, Right} \\ \text{No crosses at the center} \end{array}$$

Fig. 3c

$$\tilde{X}^{(3)}(t) = 3 \begin{array}{c} \text{Diagram 1} \\ \text{Two nodes connected by a horizontal line. Top node has an upward arrow. Bottom node has a downward arrow. Arrows on the line point right.} \end{array} + 9 \begin{array}{c} \text{Diagram 2} \\ \text{Two nodes connected by a horizontal line. Top node has an upward arrow. Bottom node has a downward arrow. Arrows on the line point right. There is an additional node with an upward arrow and a downward arrow between the two nodes.} \end{array} + 18 \begin{array}{c} \text{Diagram 3} \\ \text{Two nodes connected by a horizontal line. Top node has an upward arrow. Bottom node has a downward arrow. Arrows on the line point right. There are two additional nodes with upward arrows and downward arrows between the two main nodes.} \end{array}$$

$$+ 3 \begin{array}{c} \text{Diagram 4} \\ \text{Two nodes connected by a horizontal line. Top node has an upward arrow. Bottom node has a downward arrow. Arrows on the line point right. There is an additional node with an upward arrow and a downward arrow between the two nodes. There is also an additional node with an upward arrow and a downward arrow to the left of the first node.} \end{array} + 9 \begin{array}{c} \text{Diagram 5} \\ \text{Two nodes connected by a horizontal line. Top node has an upward arrow. Bottom node has a downward arrow. Arrows on the line point right. There are two additional nodes with upward arrows and downward arrows between the two main nodes. There is also an additional node with an upward arrow and a downward arrow to the left of the first node.} \end{array}$$

Fig. 3d

$$\begin{array}{c} t \\ \rightarrow \\ i \end{array} \quad t_0 \quad = \quad v_i \exp[-\eta_i(t-t_0)]$$

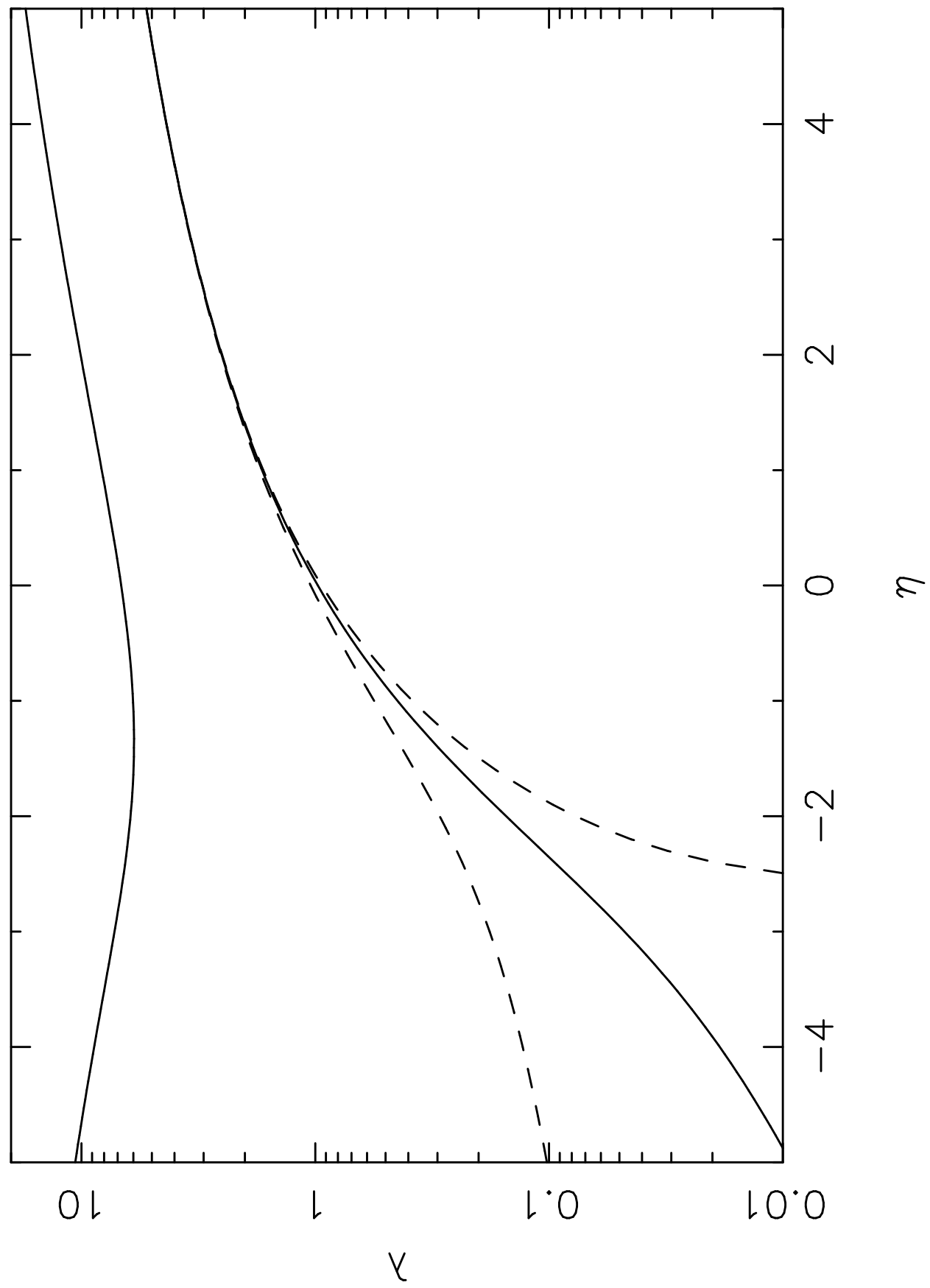
$$\begin{array}{c} t \\ \rightarrow \\ i \end{array} \quad t_0 \quad = \quad w_i(t)$$

$$t \begin{array}{c} i \\ \rightarrow \\ 1 \end{array} \begin{array}{c} j \\ + \\ k \end{array} \quad = \quad -f_{ijkl} \int_{t_0}^t dt' \exp[-\eta_i(t-t')] [\dots]$$

Fig. 4

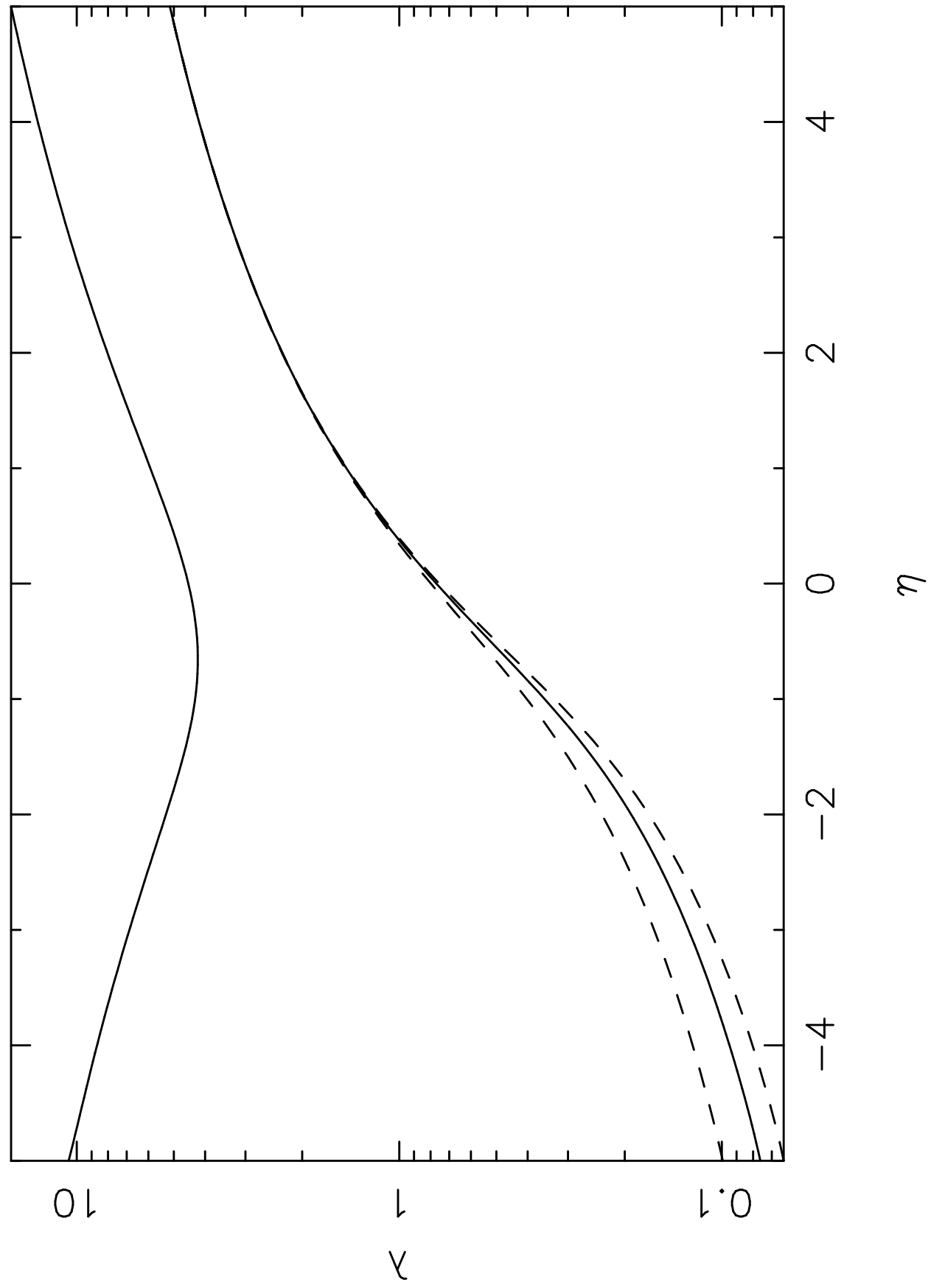
Chaturvedi & Drummond Figure 5a

Relaxation rates for $G^{(1)}$, $N = 1$



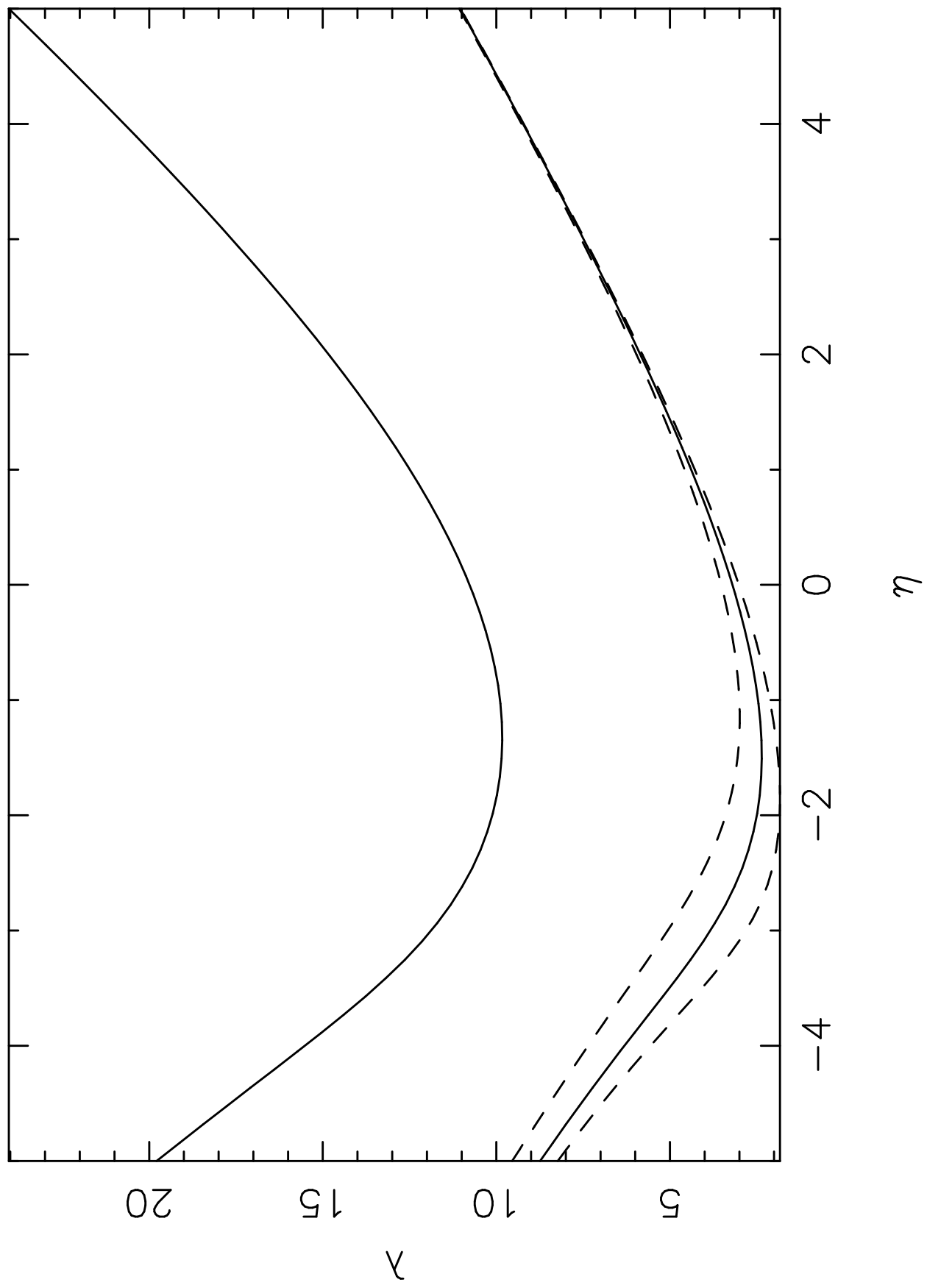
Chaturvedi & Drummond Figure 5b

Relaxation rates for $G^{(1)}$, $N = 4$

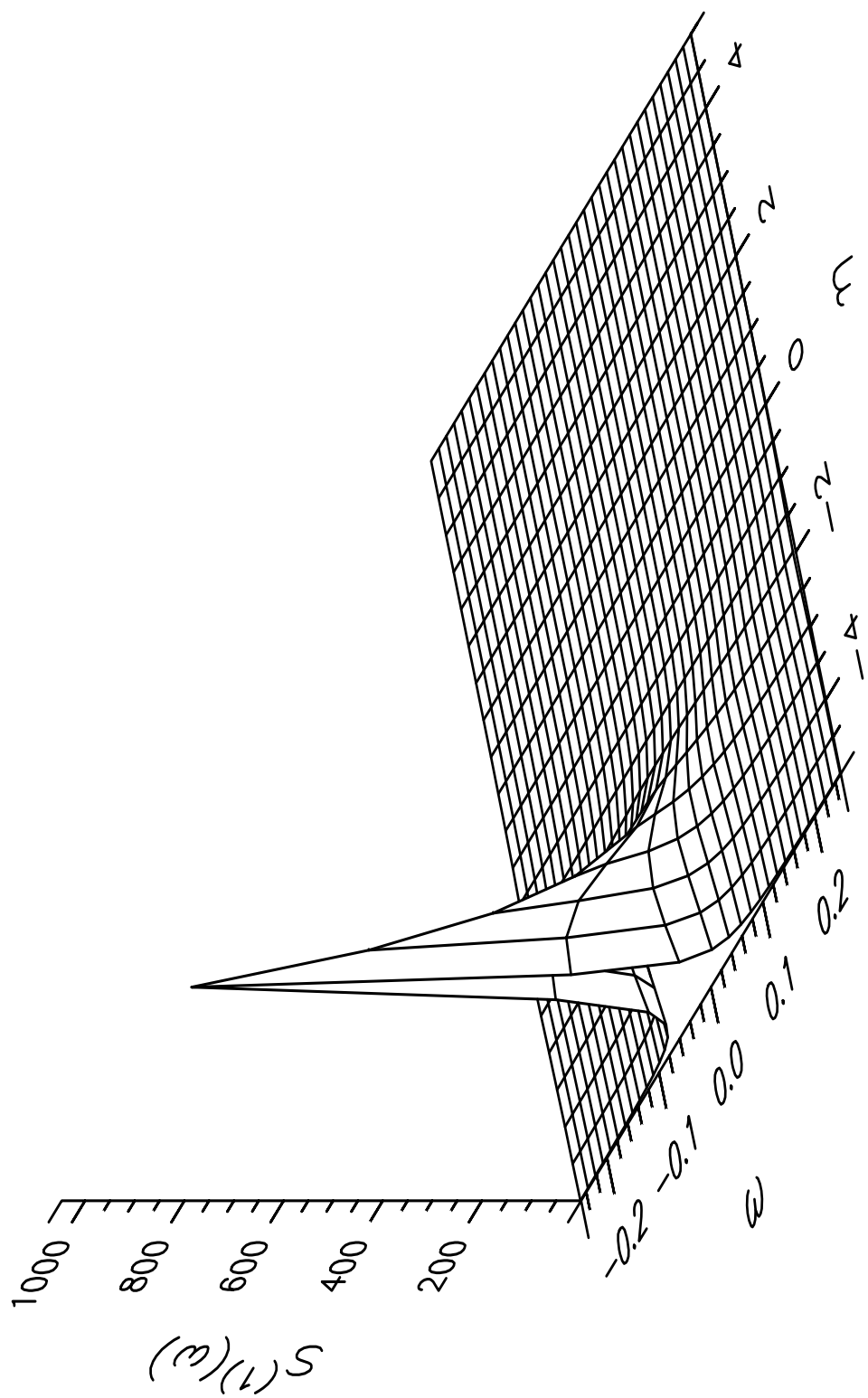


Chaturvedi & Drummond Figure 5c

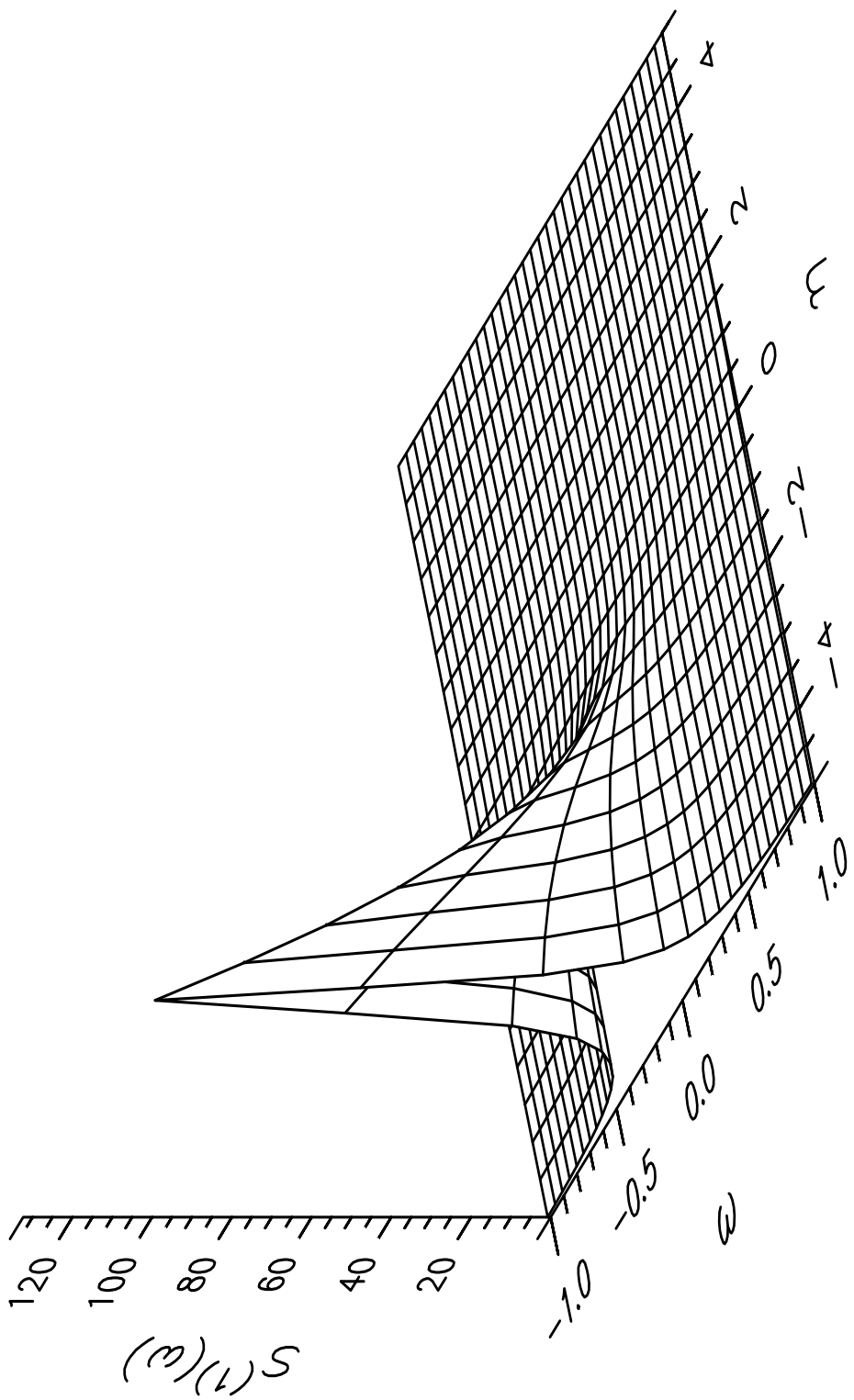
Relaxation rates for $G^{(2)}$, $N = 1$



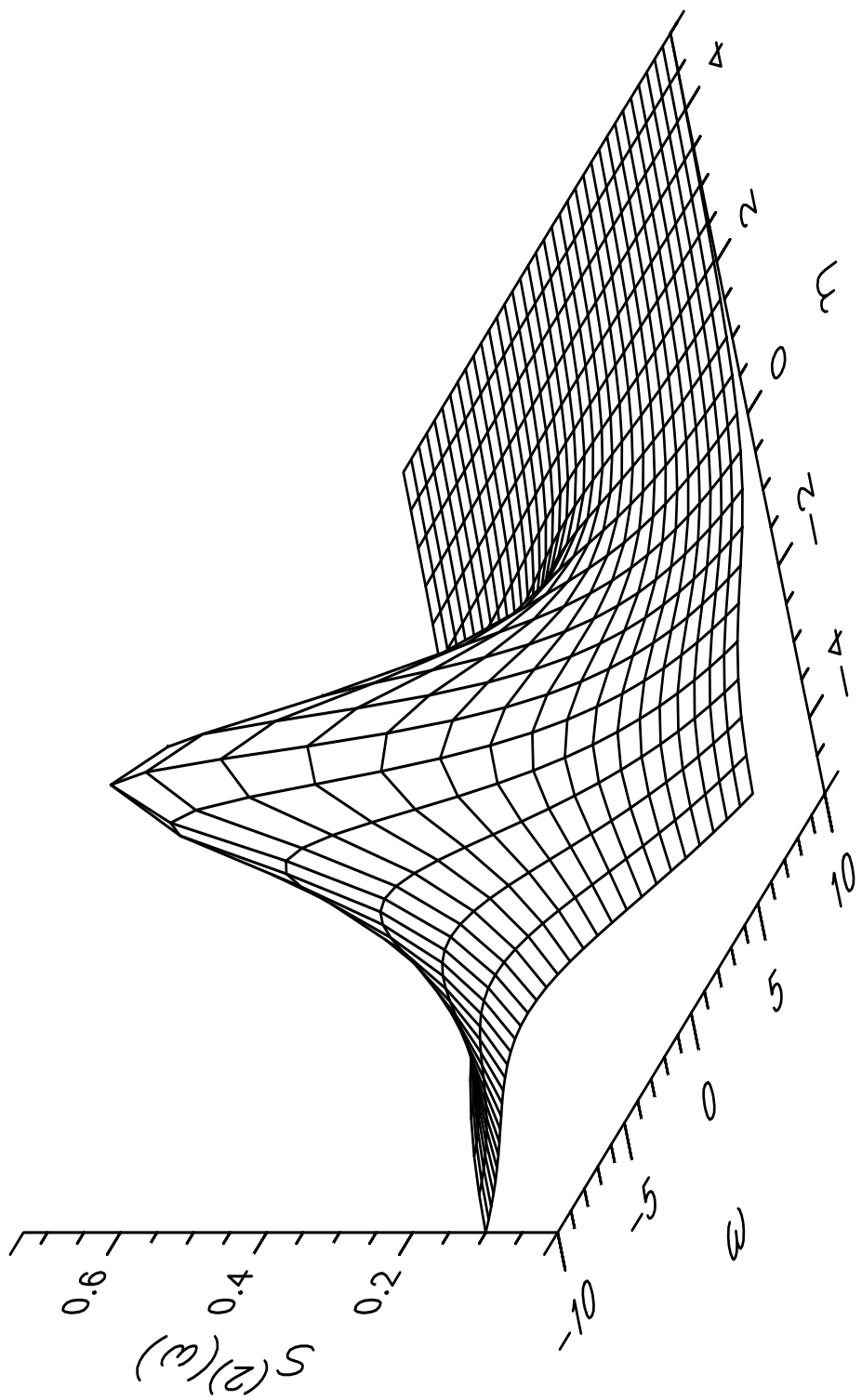
Chaturvedi & Drummond: Figure 6a
Approximate spectrum of $x(t)$ for $N = 1$



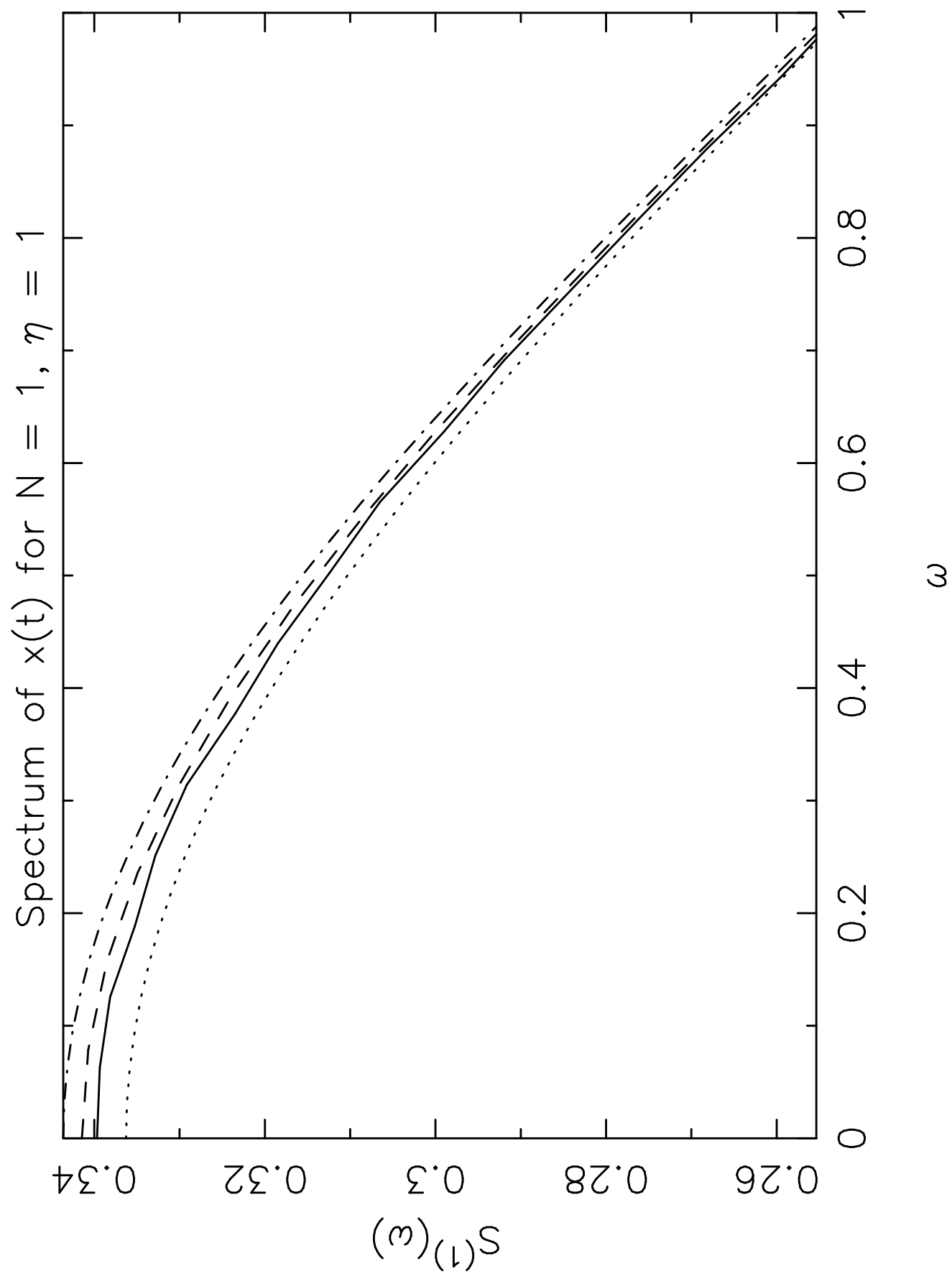
Chaturvedi & Drummond: Figure 6b
Approximate spectrum of $x(t)$ for $N = 4$



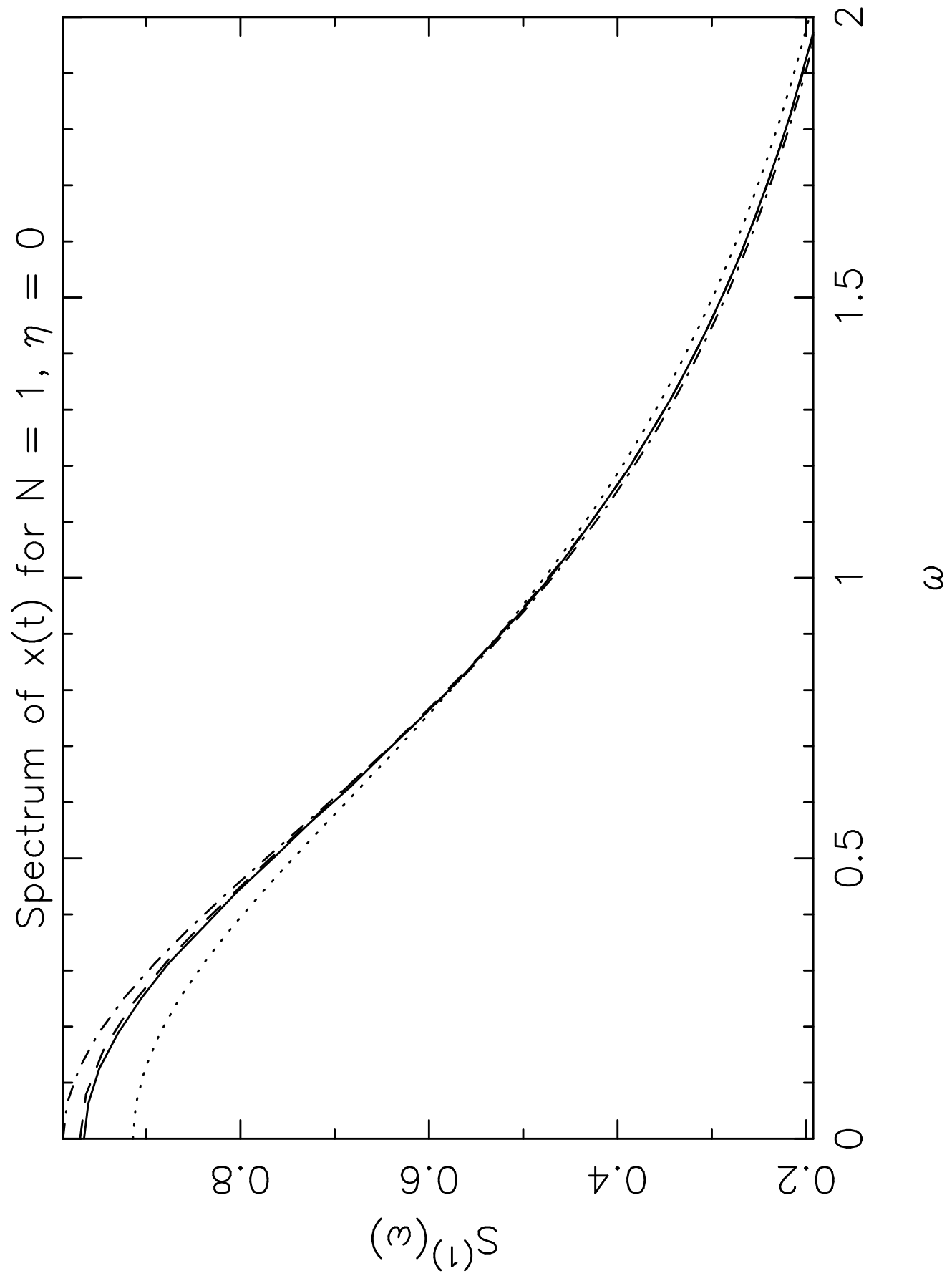
Chaturvedi & Drummond: Figure 6c
Approximate spectrum of $x^2(t)$ for $N = 1$



Chaturvedi & Drummond: Figure 7a

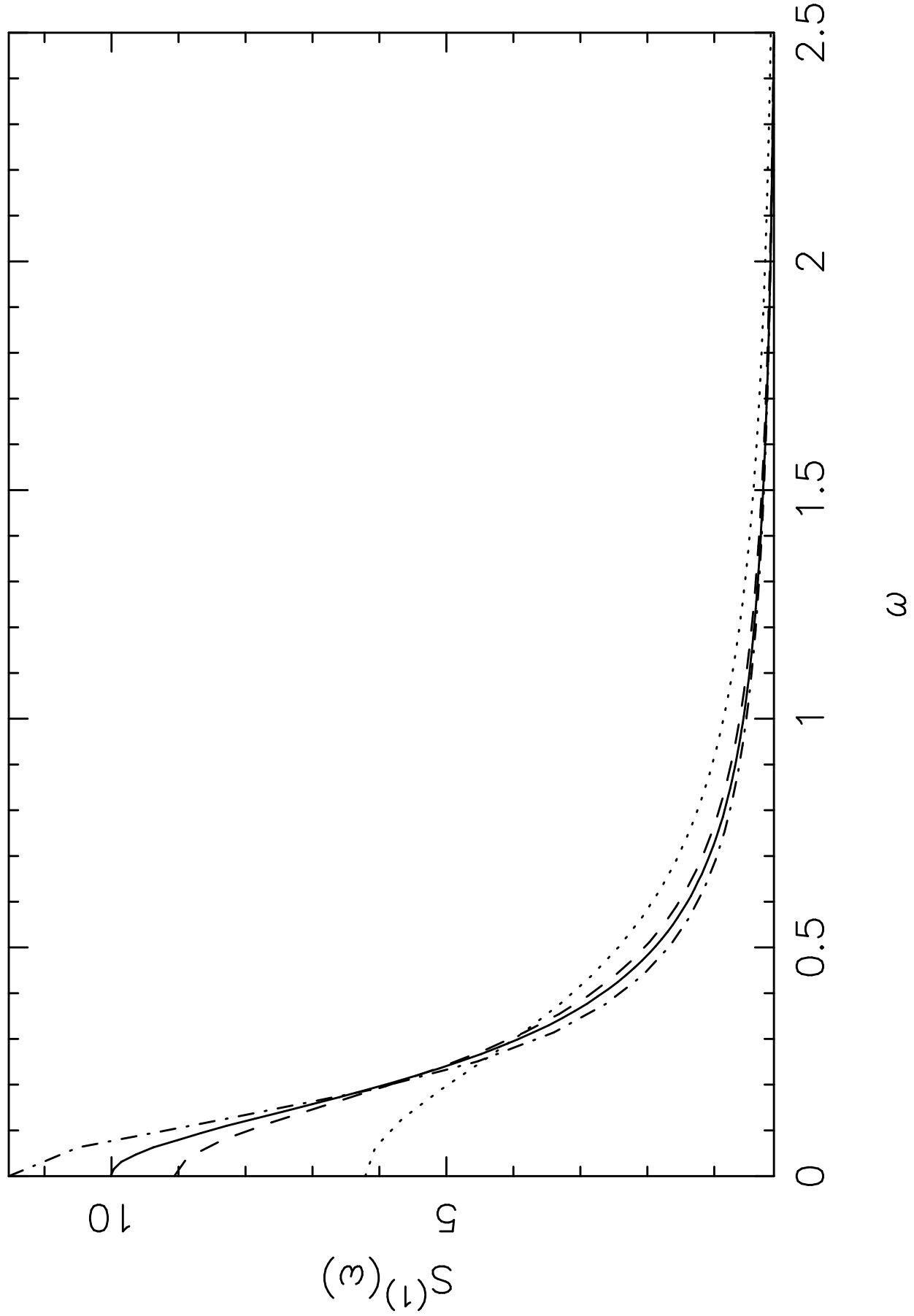


Chaturvedi & Drummond: Figure 7b

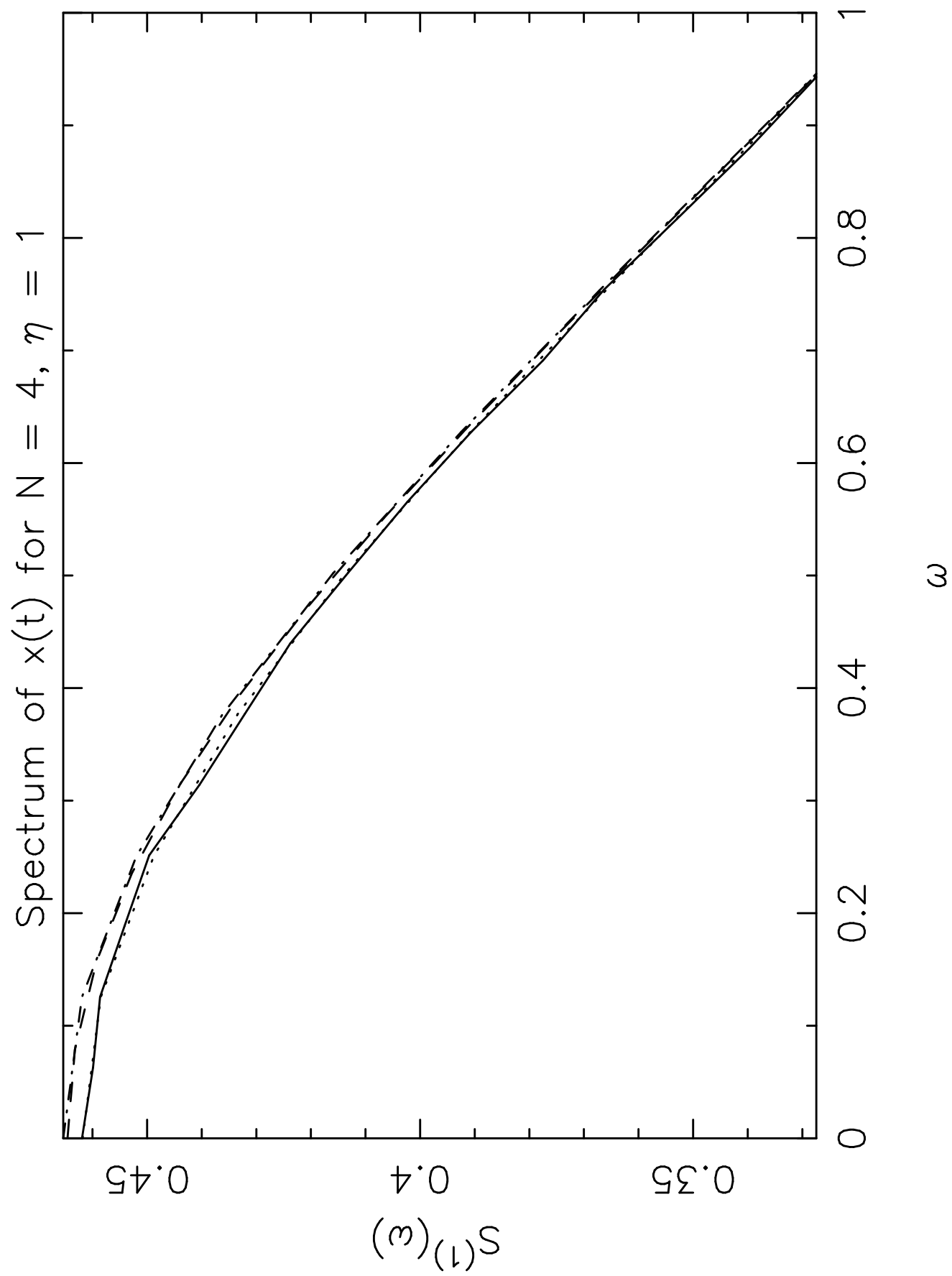


Chaturvedi & Drummond: Figure 7c

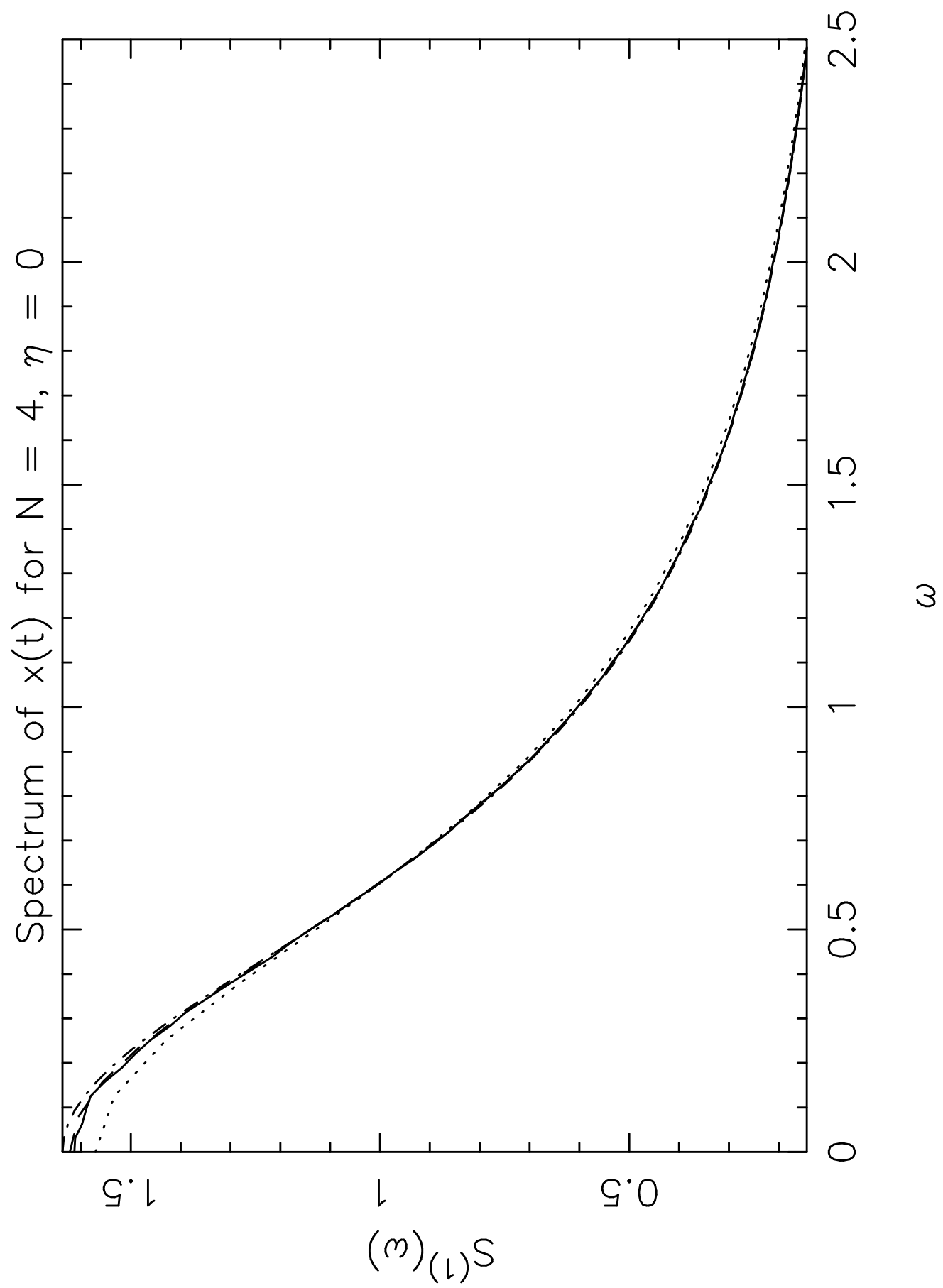
Spectrum of $x(t)$ for $N = 1, \eta = -1.5$



Chaturvedi & Drummond: Figure 8a

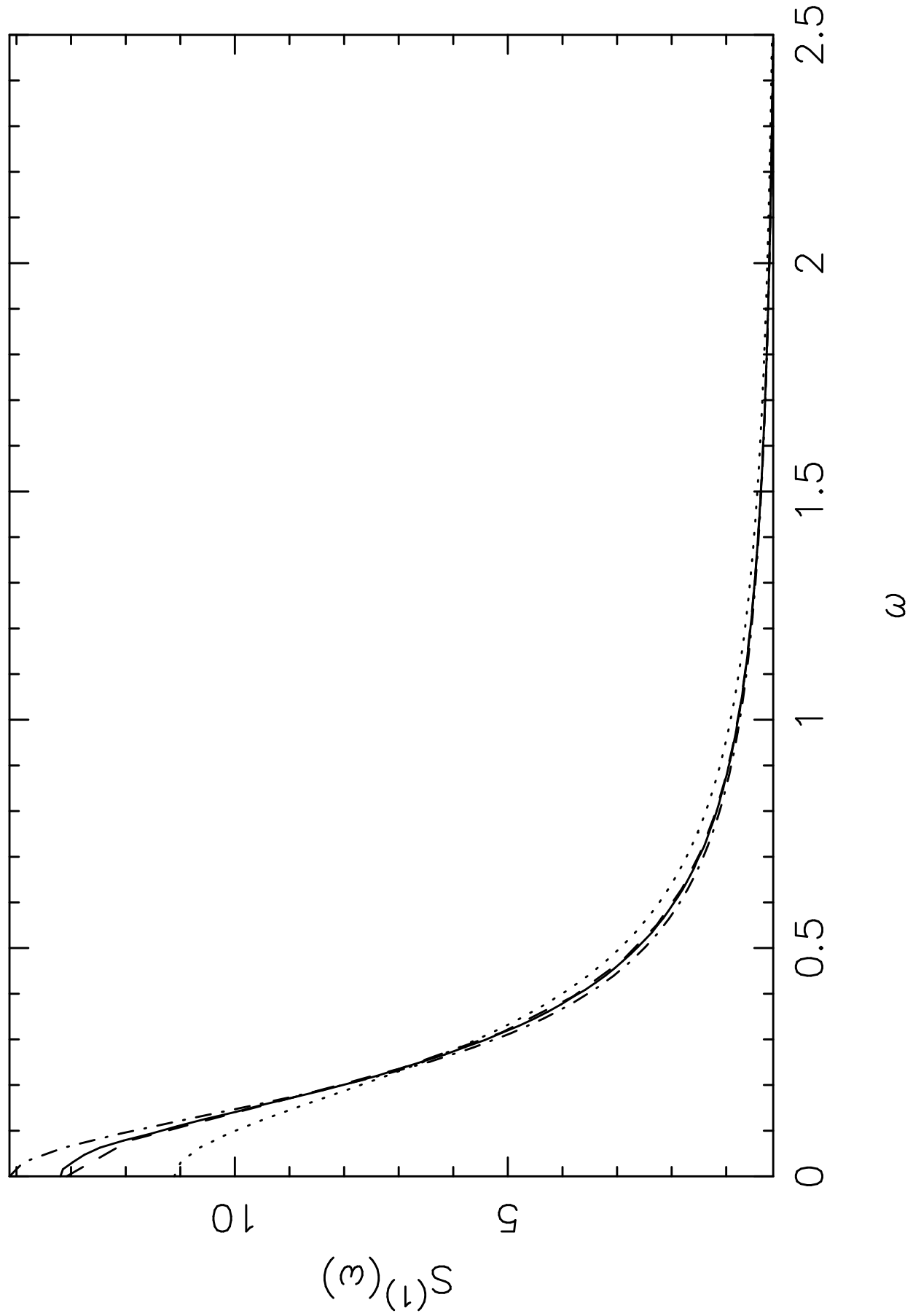


Chaturvedi & Drummond: Figure 8b

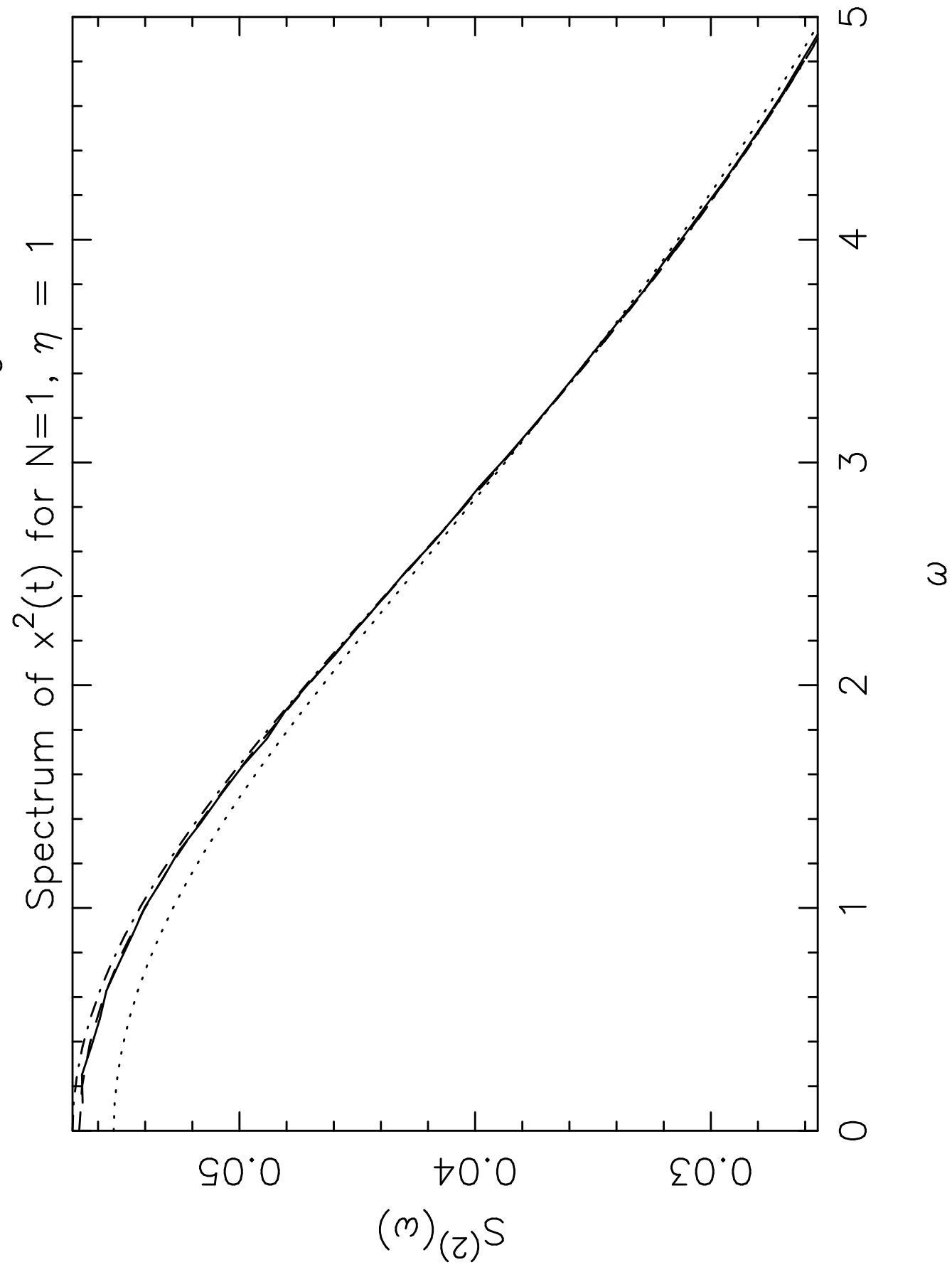


Chaturvedi & Drummond: Figure 8c

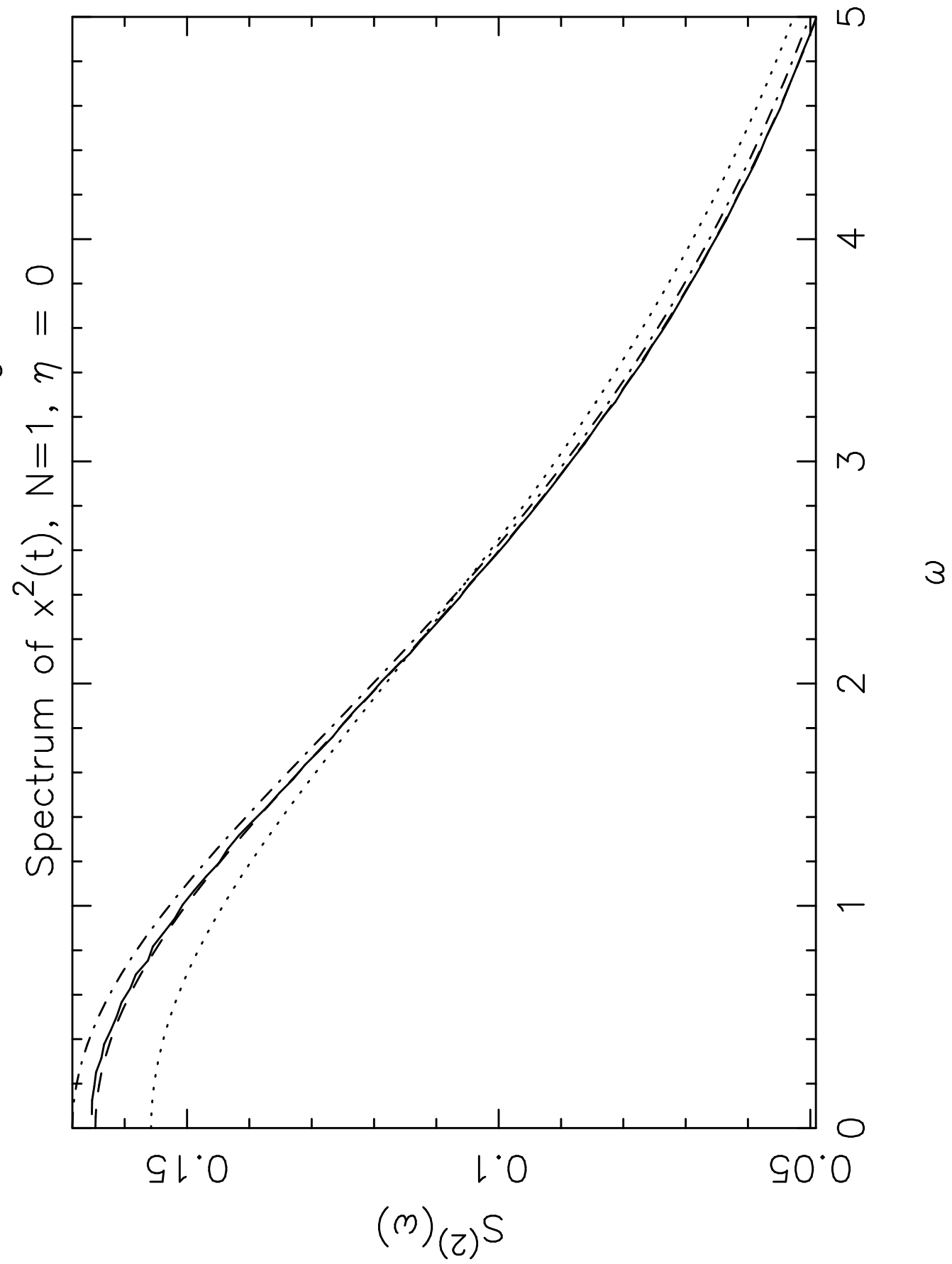
Spectrum of $x(t)$ for $N = 4$, $\eta = -1.5$



Chaturvedi & Drummond: Figure 9a

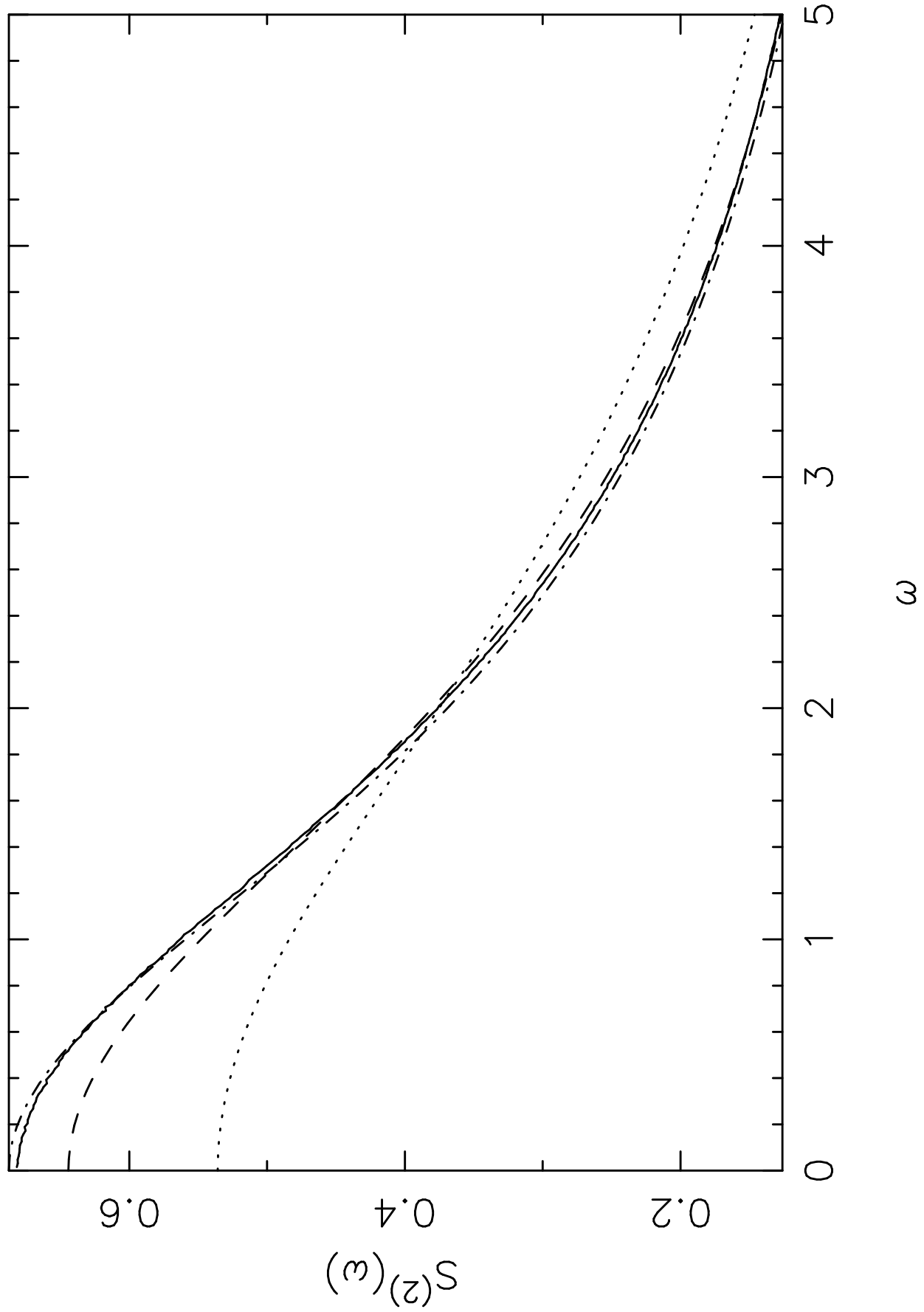


Chaturvedi & Drummond Figure 9b

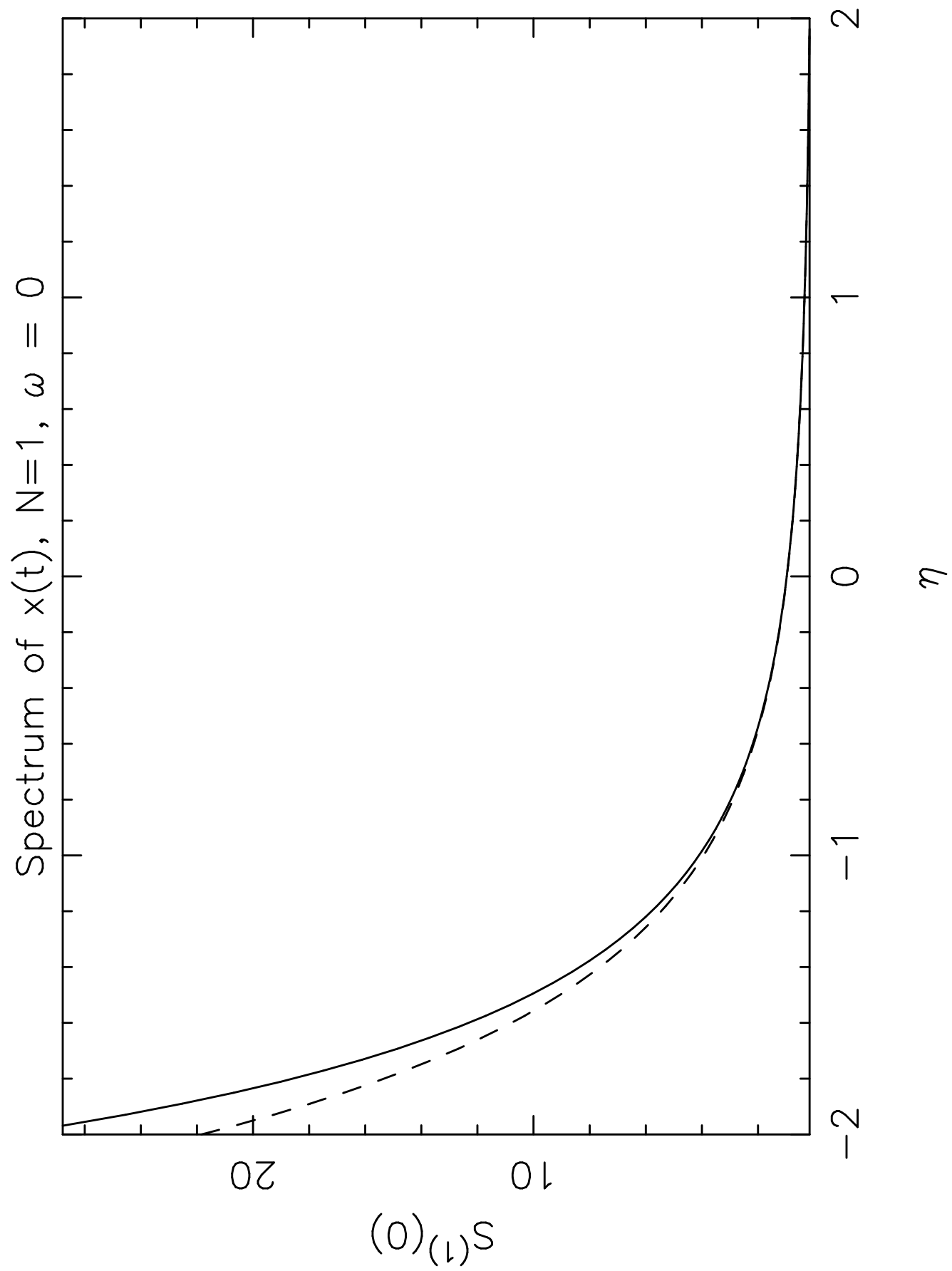


Chaturvedi & Drummond Figure 9c

Spectrum of $x^2(t)$, $N=1$, $\eta = -1.5$

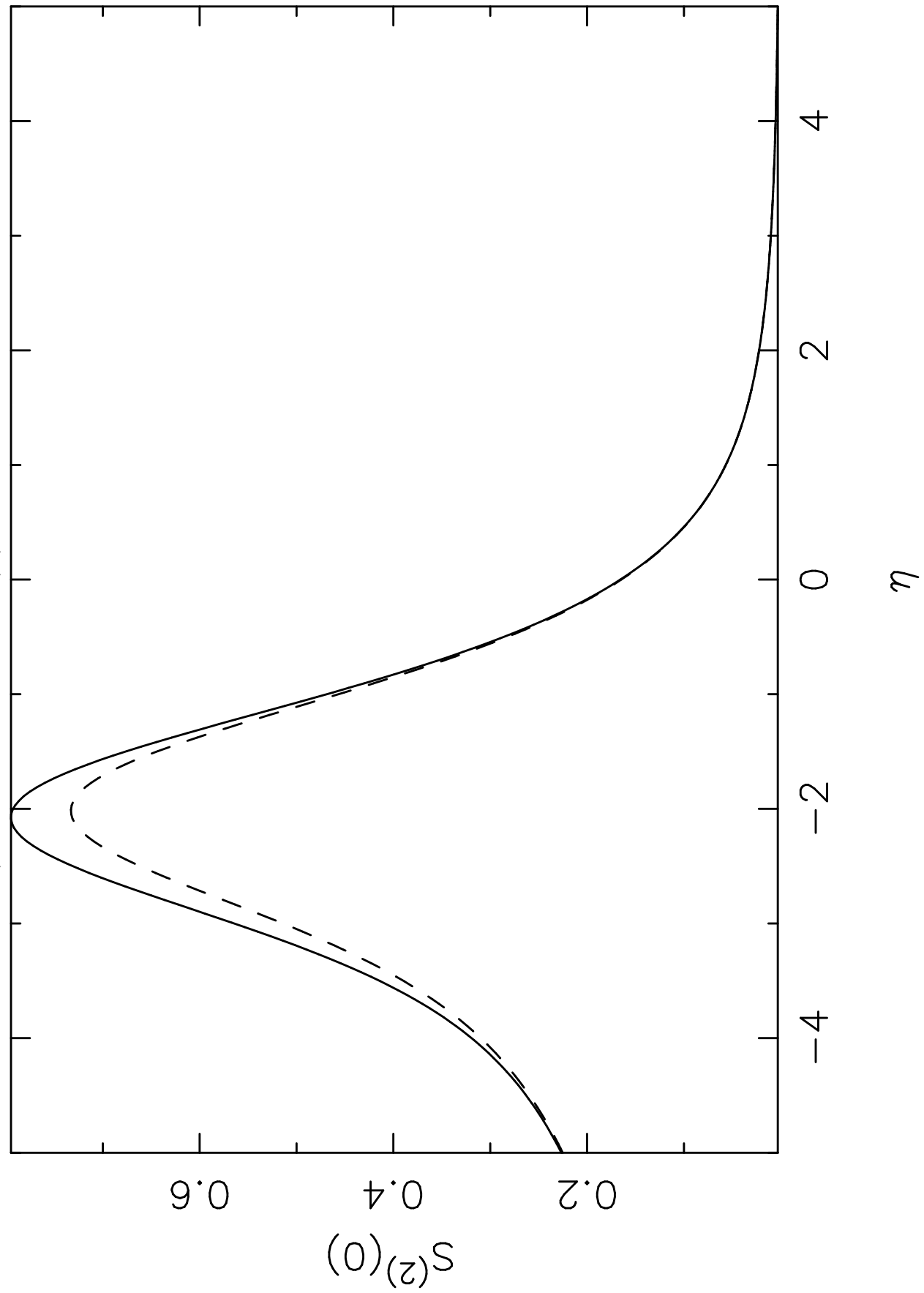


Chaturvedi & Drummond Figure 10a



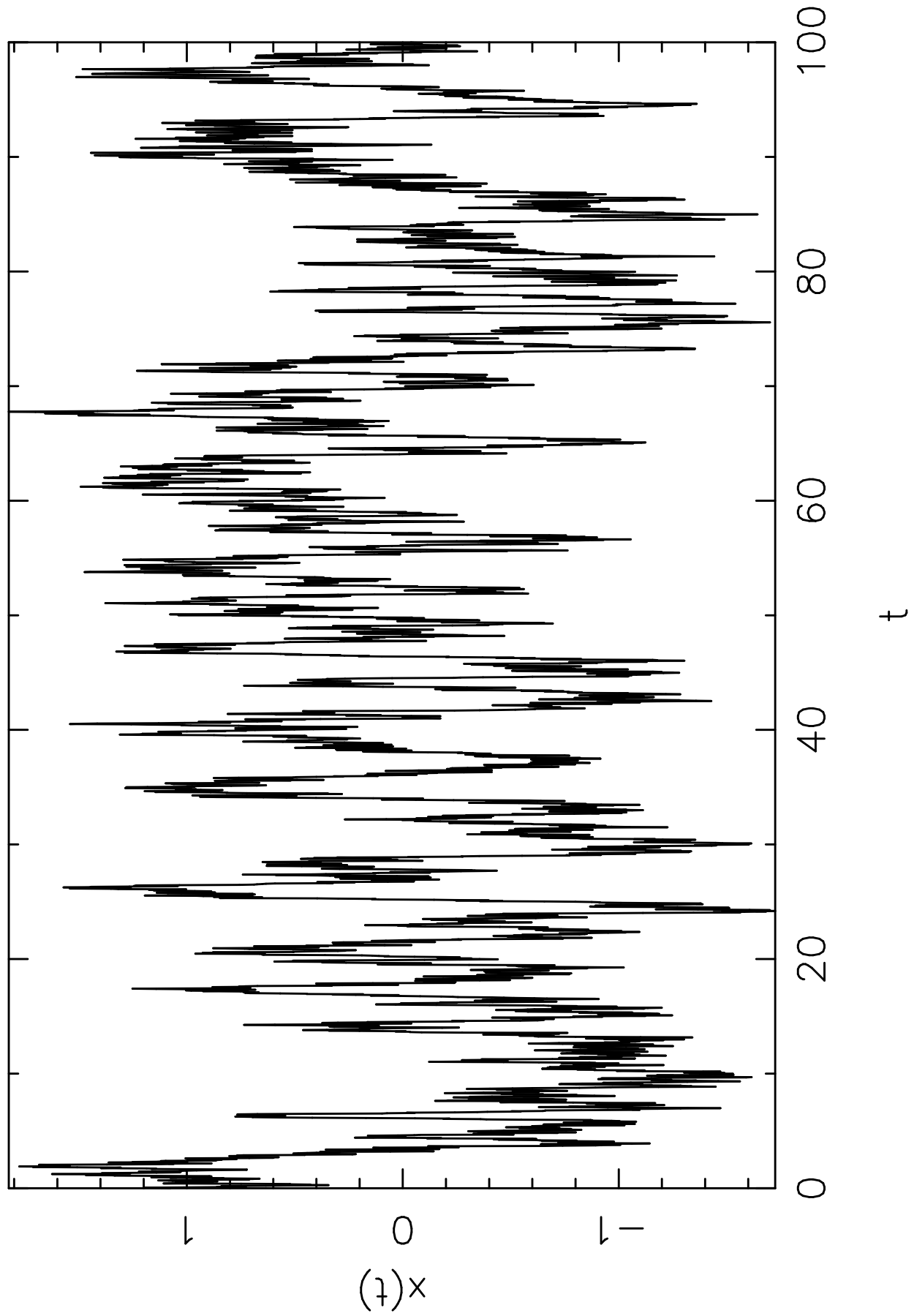
Chaturvedi & Drummond Figure 10b

Spectrum of $x^2(t)$, $N=1$, $\omega = 0$



Chaturvedi & Drummond: Figure 11

Time-evolution of $x(t)$, $N=1$, $\eta = 0$



Chaturvedi & Drummond: Figure 12

